Sigma J Eng Nat Sci, Vol. 44, No. 5, pp. 3120–3142, October, 2026

Sigma Journal of Engineering and Natural Sciences
Web page info: https://sigma.yildiz.edu.tr
DOI: 10.14744/sigma.2026.2147

Research Article

Strength optimization of low-molarity geopolymer mortars with ceramic waste powder

Aslı KESKİN[1], Mucteba UYSAL[1], Hasan DİLBAS[2], Turgay COŞGUN[3], Beyza AYGÜN[4,*]

[1]*Department of Civil Engineering, Yıldız Technical University, İstanbul, 34220, Türkiye*
[2]*Department of Civil Engineering, Kırşehir Ahi Evran University, Kırşehir, 40100, Türkiye*
[3]*Department of Civil Engineering, İstanbul University-Cerrahpaşa, İstanbul, 34098, Türkiye*
[4]*Vocational School, İstanbul Okan University, İstanbul, 34959, Türkiye*

ARTICLE INFO

Article history
Received: 25 February 2025
Revised: 04 May 2025
Accepted: 21 July 2025

Keywords:
Ceramic Waste Powder; Geopolymer Mortars; Low-Molarity; Mechanical Properties; Optimization

ABSTRACT

This study considers the production and performance of geopolymer mortars made up of 100% waste ceramic powder and 100% granulated blast furnace slag, specific for achieving the structural values through low-molarity activation. Mixtures were prepared using binder contents of 100%, 75%, 50%, and 25% by weight, activated using sodium hydroxide of 1 M, 2 M, 4 M, and 6 M molarity and sodium silicate/sodium hydroxide content ratio of 1.0, 1.5, and 2.5 and a constant activator/binder ratio of 0.7. Mortars were thermally treated in the range of 60 °C to 100 °C for 48 h and tested using ASTM, ACI, Eurocode, and British Standard tests for compressive strength, flexural strength, splitting tensile strength, direct tensile strength, elasticity modulus, porosity, unit weight, and water absorption. 75% granulated blast furnace slag+25% waste ceramic powder activatable with 6 M sodium hydroxide and 2.5 ratio and heat-treated in 100 °C gave the maximum compressive strength of 58.96 MPa. 50% granulated blast furnace slag+50% waste ceramic powder showed the most balanced mechanical profile having flexural strength of 9.84 MPa, elasticity modulus of 22.56 GPa, a tensile-to-compressive strength ratio of 0.1818 and flexural-to-compressive strength ratio of 0.8029. Curing in 80 °C was optimum in reducing the shrinkage while developing the strength while the heating in 100 °C added up the strength along with slight microcracking. ASTM predictions displayed close correlation to the experiment results while the ACI as well as the Eurocode prediction was less accurate. Multi-criteria decision-making analysis identified the 1.2% polyvinyl alcohol fiber-reinforced series as the most successful having a 24.5% increase in the compressive strength, 77.9% in flexural strength, and lowest porosity value being 20.73% along with water absorption of 10.35%. These results prove that high-strength and durable binders are reliably possible through the low-alkali activation of industrial wastes that not only provide a functional cement replacement in the structural element but also a scalable approach bridging the gap between the material innovation and the pressing need of sustainable construction.

Cite this article as: Keskin A, Uysal M, Dilbas H, Coşgun T, Aygün B. Strength optimization of low-molarity geopolymer mortars with ceramic waste powder. Sigma J Eng Nat Sci 2026;44(5):3120–3142.

***Corresponding author.**
*E-mail address: beyza.fahriye.aygun@gmail.com

This paper was recommended for publication in revised form by Editor-in-Chief Ahmet Selim Dalkilic

Published by Yıldız Technical University Press, İstanbul, Turkey
© Author. This is an open access article under the CC BY-NC license (http://creativecommons.org/licenses/by-nc/4.0/).

INTRODUCTION

Ordinary Portland Cement (OPC) has been the backbone of conventional construction for centuries. Its environmental impact is now proving unsustainable. OPC manufacturing consists of a process of calcination and clinkerization at over 1400 °C. These steps are not only very energy-intensive but also release approximately one ton of CO_2 for every ton of cement manufactured [1-3]. Collectively, this is responsible for nearly 8% of anthropogenic greenhouse gas emissions worldwide—a proportion that is continually increasing with the ever-growing needs for infrastructure and conurbations [4]. In view of this predicament, the development of alternative low carbon binder systems is not only urgent but inevitable. Some chemical improvements have been made to the performance of traditional OPC systems in the last few years. Polycarboxylate ether superplasticizer greatly enhances particle dispersion, reduces water requirement and can obtain an increase of compressive strength of over 500%. However, these additions do not lower the inherent CO_2 emissions from the standard OPC production method. In contrast, geopolymer mortars (GMs) prepared by alkali activation of aluminosilicate-rich industrial by-products have been proposed as possible replacements. These materials do not require high temperature calcination and can produce stable N-A-S-H or C-A-S-H gels at room or slightly higher temperatures [5]. Several additional precursors such as fly ash (FA) [6, 7], granulated blast furnace slag (GBFS) [8, 9], metakaolin (MK) and ceramic waste powder (CWP) have shown excellent mechanical behavior and circular economy potential [10-12]. CWP-based GMs with a curing temperature of 105 °C under low alkali mediums (11–15% Na_2O, silicate modulus < 0.3) can reach up to approximately 41 MPa compressive and approximately 10 MPa flexural strengths, as claimed by Kaya [13]. These findings are a confirmation of the feasibility of these types But alkali activator optimization is a perennial problem. Existing literature is biased toward the use of high molarity NaOH solutions (10–16M), guaranteeing a good alumina and silica dissolution. These are very limited formulations as far as their high viscosity, efflorescence, and hazard factor are concerned [14, 15]. A counterreaction is the growing literature in favor of low-molarity systems (2–6M). Kaya [13] demonstrated that while CWP–FA mixes exhibit higher microstructural stability and sulfate resistance than OPC and high-alkali geopolymers, they remain extremely sensitive to variations in activator molarity, silicate modulus, and curing temperature. Kop and Yazıcıoglu [16] found that 4M NaOH with the sodium silicate/ hydroxide ratio of 2.0 could produce compressive strengths above 60 MPa. These results underline the importance of a precise balance between NaOH and NH_4-based activator components. Kabay and Kızılkanat [17] also showed that GMs made with low-molar NaOH and sodium silicate, and based on pumice, achieve adequate mechanical strength. Their incorporation of phase change materials gave the mortars thermal buffering capability during heating and cooling, thus broadening their application from structural uses to energy-efficient construction. In addition to material developments, experimental procedures in GM research have also improved. This ideology forms the methodology in the present investigation, in which the curing temperature and the activator composition were taken as input parameters, and the mechanical and durability attributes were output responses. Al-Zwainy and Al-Marsomi [18] also adopted structural equation modeling and SmartPLS to investigate multivariable cause–and–effect relationships within regional construction programs.

Despite being increasingly acknowledged for their eco-friendliness and cost-effectiveness, the practical application of low-molarity GMs is still plagued by long-standing limitations on their mechanical performance, standardization, and compositional calibration. Contrary to OPC mortars, which are dictated by established standards like ASTM C109, EN 196-1, ACI 318, and BS 3892, there are no universally applicable testing regimes for geopolymer formulations, especially for hybrid-precursor-based systems like GBFS-WCP mixtures. Flexural strength, tensile-to-compressive strength ratios, and elastic modulus are measured erratically across studies, with differences in curing regimes, geometry of specimens, and load application yet again casting a cloud of uncertainty on cross-study comparability.

Although low-molar NaOH concentrations (1M–4M) offer clear advantages in terms of sustainability and handling compared to high-molarity NaOH, they are generally associated with basic reaction kinetics, increased porosity, and poor matrix densification, resulting in lower early-age strength and long-term structural integrity. In contrast, high-alkali systems (8M–14M) ensure rapid geopolymerization, but they suffer from serious limitations such as brittleness, poor workability, and safety-related handling issues, which further restrict their scalability. Recently, optimal enumeration of the sodium silicate/hydroxide ratio, precursor adjustment and application of moderate thermal curing temperatures such as 80°C have been shown to solve major overlaps with the facilitating low-alkali system performance by improving cohesion within the gel, slackening shrinkage levels and enhancing compressive strength levels, though still with limitations such as the present poor understanding of ultra-low molarity, ceramic dominated mortars with their 1M–2M molarities, especially with regards to susceptibility to microcracking at higher curing temperatures and partial recovery patterns within early-age hydration phases, formulating comparative insights across international standards that make design codes difficult to formulate and integrating them into mainstream construction becomes a problem even more so. Consequently, the present work proposes Multi-Criteria Decision-Support Method (MCDM)-driven mix design optimization, focused fiber-reinforcement, and a cross-standard-specific evaluation of mechanical outcomes to design aqueous-based, low-molarity GMs that are not only competent from a structural perspective and long-lasting by design but also

consistent with practical and regulative expectations for modern construction applications.

MATERIALS AND METHODS

Materials

GBFS presented a specific gravity of 2.91, Blaine fineness of 410 m^2/kg, and average particle size of about 18 μm, while CWP showed a specific gravity of 2.65 and Blaine fineness of 356 m^2/kg but a coarser average particle size of about 24 μm. Binder mixes were prepared by mixing GBFS and CWP in varied weight ratios of 100:0, 75:25, 50:50, and 25:75, whereas the total binder was kept constant at 480 kg/m^3 in all mixes. CEN sand as per TS EN 196-1 was utilized as the fine aggregate in a sand-to-binder ratio of 2.5 for uniform packing density and uniform workability. Alkaline activation was performed using the solutions of sodium hydroxide (NaOH) and sodium metasilicate (Na_2SiO_3), within Na_2SiO_3/NaOH ratios of 1.0, 1.5, and 2.5, and a constant activator-to-binder ratio of 0.7 to provide efficient geopolymerization conditions. NaOH solutions of 1 M, 2 M, 4 M, and 6 M concentration were prepared from analytical-grade pellets of NaOH (>99.1% purity), dissolving the same in distilled water and aging for 24 hours to achieve complete dissolution and stability against heating.

The chemical properties of all major constituents consisting of GBFS, WCP, NaOH, and Na_2SiO_3 are presented in the form of the chemical table in Table 1. Fiber-reinforced GMs in the optimization phase have also been developed for this present work using the fibers of basalt (BF/B) and polyvinyl alcohol fibers (PVAF/P), respectively, in volumetric fractions of 0.4%, 0.8%, and 1.2%.

The physical properties of these fibers in the form of their tensile modulus, average length, and density are presented in the form of the physical properties table in Table 2. Further, the exact weights of all the materials utilized for each cubic meter are presented in the form of the material quantification in Table 3.

Table 2. Physical properties of fibers

Properties	Basalt	PVA
Density (g/cm³)	2.8	1.3
Length (mm)	12	8
Diameter (μm)	20	39
Aspect Ratio (unitless)	600	-
Nominal Tensile Strength (MPa)	4100	1620

Table 3. Amounts of materials used in GM (for kg/m^3)

GBFS	360
CWP	120
Na_2SiO_3	240
NaOH	96
Sand	1200
BF (B) (%0.4)	11.2
BF (%0.8)	22.4
BF (%1.2)	33.6
PVAF (P) (%0.4)	5.2
PVAF (%0.8)	10.4
PVAF (%1.2)	15.6

Table 1. The chemical properties of materials

Chemical properties (%)	GBFS	CWP	Na_2SiO_3	NaOH
SiO_2	44.48	63.44	27	-
Al_2O_3	11.77	20.21	-	-
Fe_2O_3	1.12	6.39	-	-
CaO	35.27	0.67	-	-
MgO	5.29	3.14	-	-
Na_2O	0.79	0.97	8.2	-
K_2O	0.52	3.97	-	-
TiO_2	0.67	0.96	-	-
LOI	0.03	-	-	-
NaOH	-	-	-	99.1
Na_2CO_3	-	-	-	0.3
Cl	-	-	-	≤ 0.01
Al	-	-	-	≤ 0.002
Fe	-	-	≤ 0.005	≤ 0.002
SO_4	-	-	-	≤ 0.01

Methods

To provide mix design and reproducibility, the absolute volume method was utilized to determine the proportions of each component as a function of their specific gravities. Dry materials were pre-homogenized in a Hobart mixer at 140 rpm for 3 minutes. NaOH solutions (1 M–6 M) were prepared by dissolving ≥99.1% pure pellets in deionized water and allowing them to stabilize for 24 hours in sealed containers to ensure complete dissolution, as well as equilibration. These alkali solutions, adjusted to Na_2SiO_3/NaOH ratios of 1.0, 1.5, and 2.5, were progressively added to the dry mixture under continuous mixing, followed by an additional 2-minute mixing phase at 285 rpm to ensure homogeneity. Fresh mortars were cast into stainless steel molds of the dimensions 50 × 50 × 50 mm and pressed using a 50 Hz vibrating table for 30 seconds in each set and immediately sealed with polyethylene film to avoid moisture loss. All geopolymer mortars reinforced with fibers were cured under similar regimes as a function of corresponding reference mixes, namely pre-curing at 23 ± 2 °C and 90 ± 5% RH during 24 h and then thermal treatment at 60 °C, 80 °C, or 100 °C. This made it possible to exclude in comparative interpretation effects caused by curing and to isolate effects caused by type and volume of fibers only. Compressive strength was tested at the end of 72 hours using a 3000 kN test machine according to TS EN 12390-3 along with a loading rate of 0.5 MPa/s and average values derived from three specimens for each condition. Elastic modulus was experimentally found in accordance with ASTM C469 using bonded strain gauges using axial stress-strain records up to 40% of the peak load. Empirical values following the estimations of ACI 318-19, Eurocode 2, and BS EN 1992-1-1 were also calculated for comparative purposes. Using a two-direction extensometer, axial and lateral deformation readings were used to derive the value of Poisson's ratio. For the measurement of flexural strength as well as splitting tensile strength, third-point loading according to ASTM C78 was utilized along with a 100 mm support span and loading rate of 0.05 MPa/s. The estimations of tensile strength by using ACI ($f_t = 0.56\sqrt{f_c'}$) and Eurocode ($f_t = 0.3f_c'^{2/3}$) formulas have also been presented for comparison against experimental values as both these standards are commonly cited in structural design.

In this context, the GMs prepared before the addition of the fiber part and covering all series and their appropriate explanations are given in Table 4.

Table 4. GMs mix proportions and IDs

Sample ID	NaOH Molarity (M)	Na_2SiO_3/NaOH Ratio	GBFS (kg/m³)	CWP (kg/m³)	Na_2SiO_3 (kg/m³)	NaOH (kg/m³)	Sand (kg/m³)
1GM1-1	1	1.0	120	360	240	96	1200
1GM1-2	1	1.0	240	240	240	96	1200
1GM1-3	1	1.0	360	120	240	96	1200
1GM1-4	1	1.0	480	0	240	96	1200
1GM1,5-1	1	1.5	120	360	240	96	1200
1GM1,5-2	1	1.5	240.0	240.0	240	96	1200
1GM1,5-3	1	1.5	360.0	120.0	240	96	1200
1GM1,5-4	1	1.5	480.0	0.0	240	96	1200
1GM2.5-1	1	2.5	120.0	360.0	240	96	1200
1GM2,5-2	1	2.5	240.0	240.0	240	96	1200
1GM2,5-3	1	2.5	360.0	120.0	240	96	1200
1GM2,5-4	1	2.5	480.0	0.0	240	96	1200
2GM1-1	2	1.0	120.0	360.0	240	96	1200
2GM1-2	2	1.0	240.0	240.0	240	96	1200
2GM1-3	2	1.0	360.0	120.0	240	96	1200
2GM1-4	2	1.0	480.0	0.0	240	96	1200
2GM1,5-1	2	1.5	120.0	360.0	240	96	1200
2GM1,5-2	2	1.5	240.0	240.0	240	96	1200
2GM1,5-3	2	1.5	360.0	120.0	240	96	1200
2GM1,5-4	2	1.5	480.0	0.0	240	96	1200
2GM2,5-1	2	2.5	120.0	360.0	240	96	1200
2GM2,5-2	2	2.5	240.0	240.0	240	96	1200
2GM2,5-3	2	2.5	360.0	120.0	240	96	1200

Table 4. GMs mix proportions and IDs (continued)

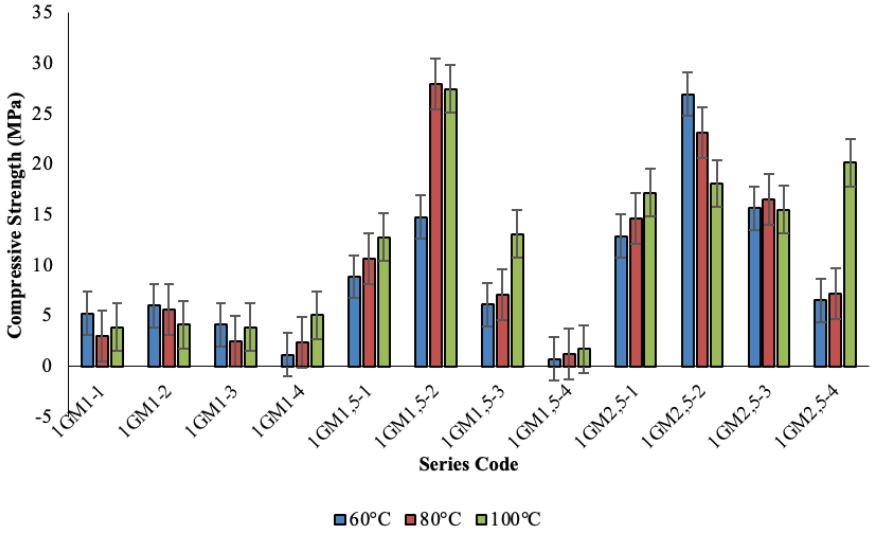
Sample ID	NaOH Molarity (M)	Na_2SiO_3/NaOH Ratio	GBFS (kg/m^3)	CWP (kg/m^3)	Na_2SiO_3 (kg/m^3)	NaOH (kg/m^3)	Sand (kg/m^3)
2GM2,5-4	2	2.5	480.0	0.0	240	96	1200
4GM1-1	4	1.0	120.0	360.0	240	96	1200
4GM1-2	4	1.0	240.0	240.0	240	96	1200
4GM1-3	4	1.0	360.0	120.0	240	96	1200
4GM1-	4	1.0	480.0	0.0	240	96	1200
4GM1,5-1	4	1.5	120.0	360.0	240	96	1200
4GM1,5-2	4	1.5	240.0	240.0	240	96	1200
4GM1,5-3	4	1.5	360.0	120.0	240	96	1200
4GM1,5-4	4	1.5	480.0	0.0	240	96	1200
4GM2,5-1	4	2.5	120.0	360.0	240	96	1200
4GM2,5-2	4	2.5	240.0	240.0	240	96	1200
4GM2,5-3	4	2.5	360.0	120.0	240	96	1200
4GM2,5-4	4	2.5	480.0	0.0	240	96	1200
6GM1-1	6	1.0	120.0	360.0	240	96	1200
6GM1-2	6	1.0	240.0	240.0	240	96	1200
6GM1-3	6	1.0	360.0	120.0	240	96	1200
6GM1-4	6	1.0	480.0	0.0	240	96	1200
6GM1,5-1	6	1.5	120.0	360.0	240	96	1200
6GM1,5-2	6	1.5	240.0	240.0	240	96	1200
6GM1,5-3	6	1.5	360.0	120.0	240	96	1200
6GM1,5-4	6	1.5	480.0	0.0	240	96	1200
6GM2,5-1	6	2.5	120.0	360.0	240	96	1200
6GM2,5-2	6	2.5	240.0	240.0	240	96	1200
6GM2,5-3	6	2.5	360.0	120.0	240	96	1200
6GM2,5-4	6	2.5	480.0	0.0	240	96	1200

To ensure statistical clarity and avoid potential misinterpretations due to variable entanglement—particularly the influence of fiber reinforcement overlapping with chemical or thermal effects—the experimental design followed a structured two-phase approach. In the first phase, a comprehensive set of GMs was prepared without any fiber inclusion, encompassing all combinations of NaOH molarity, Na_2SiO_3/NaOH ratios and curing temperatures. This phase enabled an isolated investigation of how these parameters individually and interactively affected mechanical properties such as compressive strength, modulus of elasticity, and tensile behavior, as well as durability-related indicators such as porosity and ultrasonic pulse velocity. The analysis of these results led to the selection of a subset of best mixes exhibiting optimal mechanical balance and durability as reference mixes for reinforcing. In the second phase, basalt and polyvinyl alcohol fibers were incorporated into these optimal formulations at three volume fractions without altering the original binder ratios, activator compositions, or curing conditions. This strict consistency in processing conditions between reinforced and unreinforced counterparts allowed the fiber-related effects to be examined in complete isolation from chemical or thermal influences.

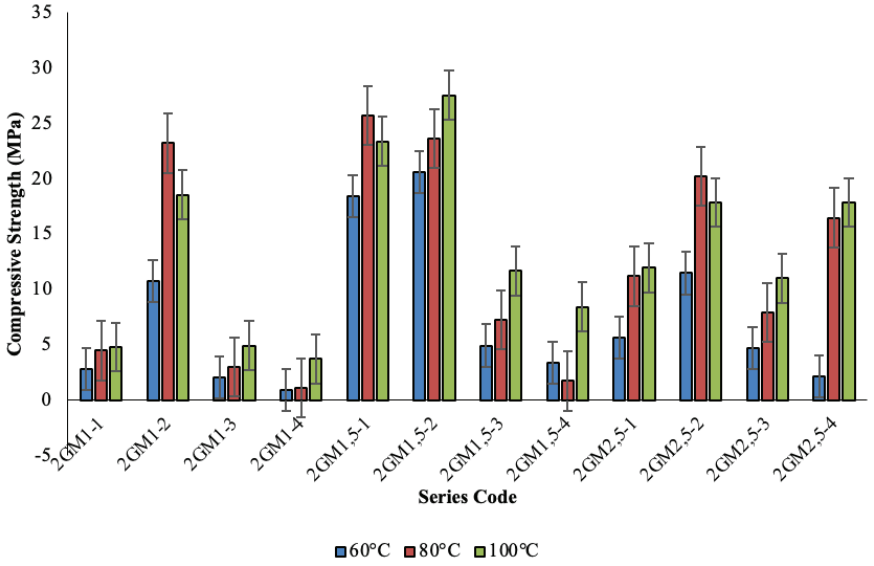
RESULTS AND DISCUSSION

Compressive Strength

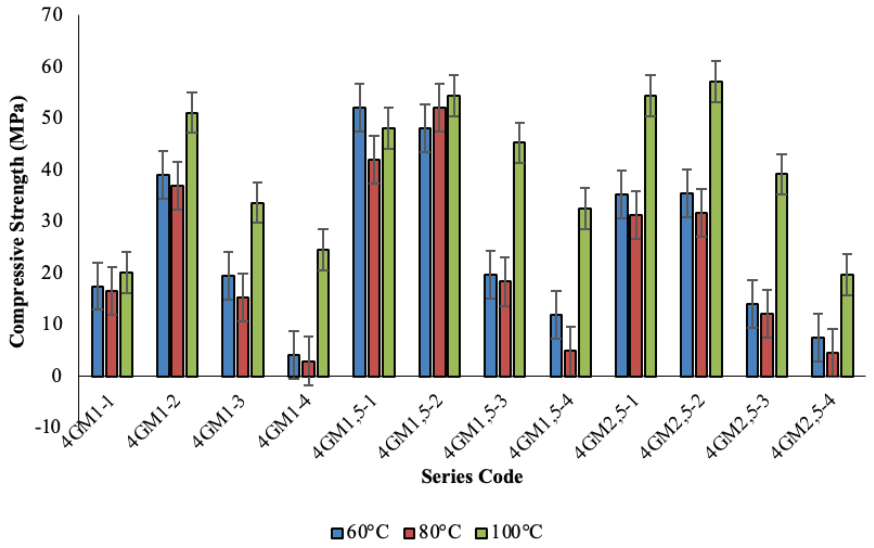
Compressive strength trends in GMs at different molarity and different curing temperatures reveal complex interactions between thermal activation, water retention, efficiency in the polymerization, and integrity in the microstructure, all having an impact on the mechanical properties of GMs (Fig. 1). 1M series follows significant variability, and 1GM1-1 follows a 41.9% reduction from 5.25 MPa at 60°C to 3.05 MPa at 80°C, and 27.5% increase to 3.89 MPa at 100°C, finally losing 25.9% from the starting point at 60°C, indicating 80°C to cause the evaporation of too much water and less efficient polymerization, and 100°C to provide some improvement through the survival of the geopolymerization reactions, albeit insufficient to recover to the


Compressive Strength (MPa)
35
30
25
20
15
10
5
0
-5
1GM1-1
1GM1-2
1GM1-3
1GM1-4
1GM1,5-1
1GM1,5-2
1GM1,5-3
1GM1,5-4
1GM2,5-1
1GM2,5-2
1GM2,5-3
1GM2,5-4
Series Code
60°C
80°C
100°C

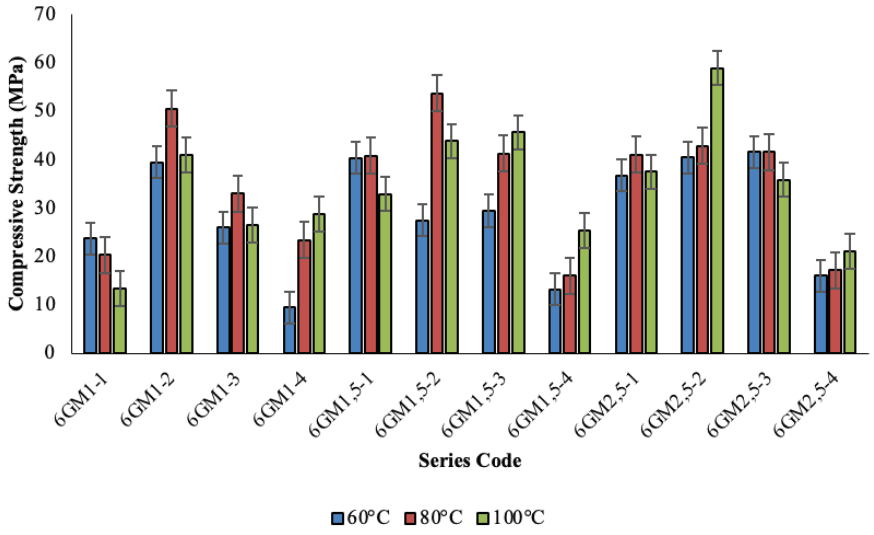
(a)


Compressive Strength (MPa)
35
30
25
20
15
10
5
0
-5
2GM1-1
2GM1-2
2GM1-3
2GM1-4
2GM1,5-1
2GM1,5-2
2GM1,5-3
2GM1,5-4
2GM2,5-1
2GM2,5-2
2GM2,5-3
2GM2,5-4
Series Code
60°C
80°C
100°C

(b)


Compressive Strength (MPa)
70
60
50
40
30
20
10
0
-10
4GM1-1
4GM1-2
4GM1-3
4GM1-4
4GM1,5-1
4GM1,5-2
4GM1,5-3
4GM1,5-4
4GM2,5-1
4GM2,5-2
4GM2,5-3
4GM2,5-4
Series Code
60°C
80°C
100°C

(c)



(d)

Figure 1. Compressive strengths of GMs prepared with different low-molarities and Na_2SiO_3/NaOH and mixing ratios.

starting point. A trend, albeit greater, follows in 1GM1-2, losing 7.4% initially from 6.06 MPa at 60°C to 5.61 MPa at 80°C, and dropping 26.2% to 4.14 MPa at 100°C, resulting in net 31.7% reduction in the overall strength, indicating the formulation to suffer from significant dehydration effects at the high-temperature side, leading to shrinkage, greater pore content, and less integrity in the matrix, making the mechanical properties weaker. 1GM1-3, in contrast, follows an initial 39.6% reduction from 4.17 MPa at 60°C to 2.52 MPa at 80°C, and unlike the above mixes, recovering significantly at 100°C, by 54.4% to 3.89 MPa, finally ending up losing only 6.7% overall from 60°C, indicating the mixture to have greater rehydration capacity at the high-temperature side, to recover some of the strength through the side-reactions in the polymerization, possibly having proceeded despite the high-temperature condition.

Completely different trend is seen in 1GM1-4, beginning at 1.18 MPa at 60°C and climbing steeply by 104.2% to 2.41 MPa by 80°C, and by the succeeding 112.0% to 5.11 MPa by 100°C, for the total 333.0% increase in strength, indicating this mixture profits significantly from the high-temperature curing through the activation of the binder and improved geopolymerization kinetics, leading to improved densification and maturation of the structure in the matrix. 1GM1,5-1, take off 8.91 MPa by 60°C, follows the pattern of a more controlled buildup in the trend, climbing by only 19.6% by 80°C to 10.66 MPa, and by the succeeding 20.2% to 12.82 MPa by 100°C, to the total 43.8% increase in the strength, indicating the improved capacity in retaining the water at the high-temperature, minimizing the shrinkage effect while allowing the retention of the polymerization, and so to the improved mechanics without the steep loss seen in the case of the poor mixes. For the 2M series, the trend follows the pattern of the steady increase in the strength, particularly by 80°C, confirming the theory that the increase in alkalinity promotes the chemical reactions to increase the strength and reduces the adverse effect from the heat leading to the loss in the water content relative to the 1M series. For instance, the 2GM1-1 series improved considerably by 60.0% at 2.80 MPa at 60°C and 4.48 MPa at 80°C, and by the succeeding 7.8% at 4.83 MPa at 100°C, to the total increase in the strength by 72.5%. This suggested the mixture gained from the intermediate heat treatment, the increase in the strength being the most at 80°C and only the marginal additional gain added at 100°C, presumably because the water content reduces at the increase in the temperature.

This is clearer in 2GM1-2, having 115.7% increase from 10.77 MPa at 60°C to 23.23 MPa at 80°C and 20.1% reduction to 18.55 MPa at 100°C, resulting in net 72.2% increase from the beginning, confirming 80°C to be the optimum temperature to cure this mixture, and 100°C to cause the shrinkage and evaporation of water, leading to some reduction in the strength, possibly through the generation of microcracks. 2GM1-3 series shows smooth and regular buildup, having 47.1% increase from 2.06 MPa at 60°C to 3.03 MPa at 80°C, and 63.0% at 100°C to 4.94 MPa, resulting in the net 139.8% gain, indicating the mixture to be extremely reactive to the increase in the curing temperature, allowing longer-term polymerization and better mechanical integrity through greater densification in the matrix. 2GM1-4 mixture, starting from the lowest beginning at 0.96 MPa at 60°C, also shows the same trend in dependence to the high-temperature condition, having 14.6% increase at 80°C to 1.10 MPa, and whopping 239.1% increase to 3.73 MPa at 100°C, resulting in the net 288.5% gain in the strength, confirming the formulation to attain the optimum only through long-term high-temperature

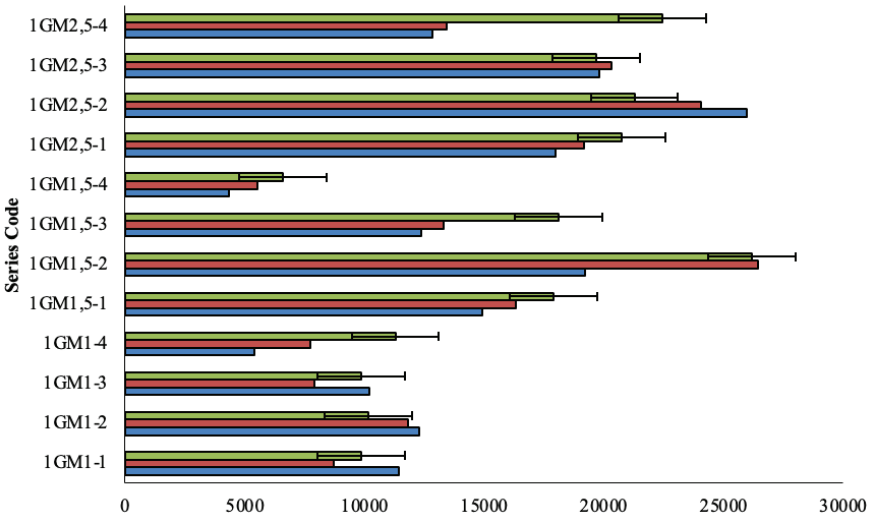
conditioning, possibly through the slow rate of the geopolymerization at the low-temperature condition. 4M and 6M series also provide some clues to the effect of the increase in alkalinity in the efficiency in thermal curing, the 4M series tending to show the most regular and smooth buildup in all the temperatures, and the 6M series having mixed responses depending on the formulation.

4GM1-1 grows by 14.6% at 80°C to 23.05 MPa and another 16.4% at 100°C to 26.85 MPa, a total 33.6% increase, reflecting greater increase in temperature to steadily increase the polymerization, leading to tighter matrix and greater load-bearing capacity. Likewise, 4GM1-2 also develops in good developing trend, 16.3% at 80°C and another 12.8% at 100°C, to 50.78 MPa, confirming the benefit of thermal curing, whereby the increase in the strength tapers off at the greater temperature. 4GM1-3, by contrast, first reduces at 80°C and recuperates at 100°C, reflecting the first shrinkage and the later-stage secondary polymerization. 6M series, by contrast, gives a less consistent trend, 6GM1-1 having a spectacular 43.7% reduction in the strength by 100°C, confirming the harmful effect of high alkalinity and high-temperature curing, leading to microcracking and water evaporation, and 6GM1-4 having a 202.8% total increase in the strength, reflecting some mixes in requiring forceful thermal curing to achieve the total geopolymerization. The highest strength series, 4GM1.5-1 and 6GM1.5-1, demonstrated initial increments of strength, slight reductions at 80°C due to shrinkage, and later 100°C recoveries, revealing binder aggregate synergy at prolonged curing. For lower molarities (1M–2M), the absence of hydroxide ions prevented full activation of the GBFS and the CWP, leaving these gels weakly cross-linked, prone to moisture losses, and shrinkage-driven porosity when exposed to elevated temperatures. Conversely, ~80°C curing attains a balance of the thermal-chemical conditions which promotes matrix densification and polycondensation without the initiation of microcracks. Although higher molarities (4M–6M) encourage geopolymerization, exceeding the thermal thresholds (high temperatures higher than 80°C) can mean stress-driven structural failure. Such tendencies reflect the nonlinear relationship of the molarity, temperature, the activation energy, and the kinetics of the humidity, as the recent literature attests.

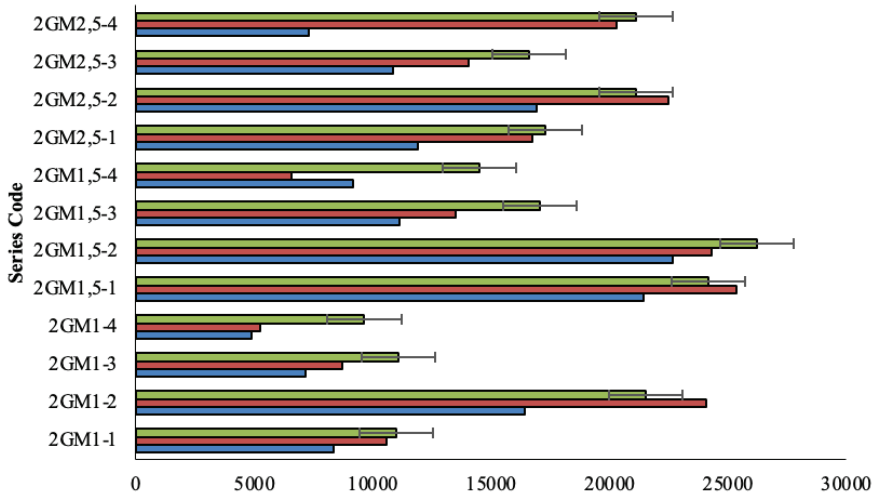
Kumar et al. [19] demonstrated that 4M and 6M NaOH-activated systems gained significant strength at only high curing conditions since ambient curing would not be able to overcome kinetic inhibitors. Likewise, Kaya [13] reported a non-linear effect between compressive strength and curing temperature for CWP-based systems, as superior strength values of 41.5 MPa were achieved at 80–105 °C, but microstructural instability at high silicate concentrations occurred upon higher heat exposure. Zhang et al. [12] verified that CWP addition in BFS-based matrix affected strength evolution through dynamic changes in Si/Al and Ca/Si ratios, whereby early-age strength would be restrained due to delayed reactivity but increased thereafter through controlled curing. Bilondi et al. [20] also proved through response surface methodology that curing at 100 °C would be ideal for achieving optimum mechanical performance only when $NaOH/Na_2SiO_3$ and solution-to-binder ratios were finely optimized—otherwise, the strength and strength loss due to porosity would ensue through chemical-heat unbalance.

Modulus of Elasticity

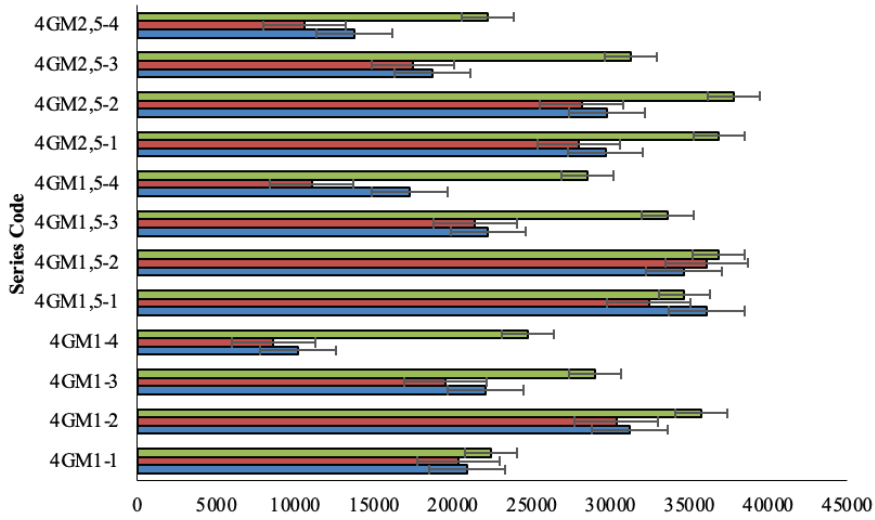
Elastic modulus trends in GMs at various molarity and curing temperature regimes reveal mechanical stiffness progression under different thermal regimes, indicating significant impacts by the efficiency of polymerization, water evaporation, shrinkage, and matrix densification (Fig. 2). 1M series manifests major stiffness declines at 80°C in some specimens through water-driven shrinkage but



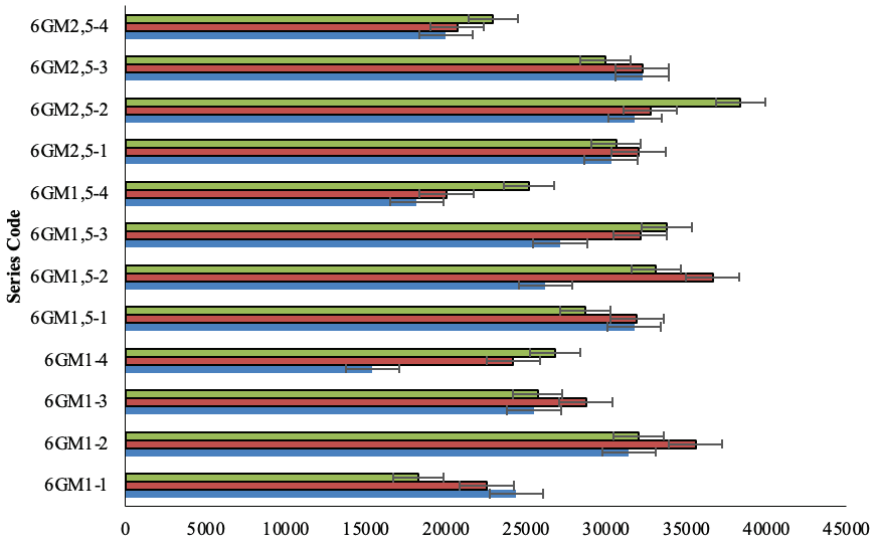
(a)



(b)



(c)



(d)

Figure 2. Elasticity modulus of GMs prepared with different low-molarities and Na_2SiO_3/NaOH and mixing ratios.

recovers to some extent at 100°C in others, indicating the necessity to provide longer thermal treatments to the lower-molarity GMs to achieve optimal structure rigidization. 1GM1-1 begins at 11.456 GPa at 60°C, declines by 23.8% to 8.732 GPa at 80°C, and later by 12.9% to 9.861 GPa at 100°C, finally resulting in 13.9% net reduction, indicating the shrinkage at the beginning reduces the stiffness, but longer heating encourages some reorganization in the aluminosilicate gel, resulting in partial restoration in the stiffness. Likewise, 1GM1-2 reduces from 12.308 GPa at 60°C to 11.842 GPa at 80°C (-3.8%) before incurring a steep 14.1% reduction to 10.173 GPa at 100°C, resulting in net 17.3% reduction in the modulus, affirming the water evaporation at high-temperature regimes to cause the introduction of discontinuities in the matrix, resulting in the reduction in elastic character despite the retention in the moderation in the strength. However, 1GM1-3 traces a different pattern, reducing by 22.3% from 10.210 GPa at 60°C to 7.937 GPa at 80°C, and recovering by 24.2% at 100°C to 9.861 GPa, resulting in only 3.4% total reduction in the stiffness, affirming some specimens shrink at intermediate regimes, and the rigidization comes back through the effect of the secondary polymerization at 100°C. The most pronounced increase is in the case of 1GM1-4, starting from 5.431 GPa by 60°C, rising by 42.9% by reaching 7.762 GPa by 80°C, and rising by another 45.6% by reaching 11.302 GPa by 100°C, reaching the whopping figure by 108.1% total gain in the modulus, confirming the mixture to be greatly based on the high-temperature curing to achieve the optimum structure, possibly because the lowered kinetics under lowered temperature.

Alternatively, the mixture 1GM1-5-1 starts by 14.924 GPa by 60°C, rising by 9.4% by reaching 16.324 GPa by 80°C, rising by another 9.7% by reaching 17.902 GPa by 100°C, recording the steady figure by 20.0% gain in the modulus, confirming the mixture to achieve the same buildup in all the temperatures by the effect of the polymerization and balanced humidity retaining capacity. In the 2M, the trend follows the same in the case of the tougher mixes, recording less steep declines and greater sensitivity to the high-temperature curing. In the 2GM1-1, while at 60°C, 13.345 GPa, rising by 13.6% by reaching 15.156 GPa by 80°C and rising by 2.4% by reaching 14.787 GPa by 100°C, achieving the net gain by 10.8% and confirming the optimum at 80°C, and causing minimum microcracking or slackening at 100°C. Similarly, 2GM1-2 rose by 17.8% by reaching 17.921 GPa by 15.219 GPa and 80°C and remained steady at 17.809 MPa by 100°C, resulting the total gain by 17.0%, confirming the mixture to maintain the worth at all the temperatures and to provide greater heat resistance and efficiency at all the processes by the effect of the polymerization.

In contrast, 2GM1-3 follows progressive improvement, from 10.874 GPa at 60°C, up 23.1% to 13.390 GPa at 80°C, and further up 14.6% to 15,345 MPa at 100°C, achieving a 41.1% overall gain, confirming that slow-stage polymerization and further densification at 100°C are the reasons for improved rigidity. Most spectacular gain in modulus comes in 2GM1-4, from 6.218 GPa at 60°C, up 87.6% to 11.671 GPa at 80°C, and further up 21.4% to 14.168 GPa at 100°C, achieving a 127.8% gain, confirming that the mixture needs to be subjected to extreme thermal curing to achieve optimal stiffness because the rate of early-stage polymerization is slow. 4M and 6M series are found to retain the modulus in a steady manner, the 4M series having consistent gain in stiffness at all the temperatures, while the 6M series gives mixed responses based on the formulation, the 4GM1-1 begins at 18.512 GPa at 60°C, up 11.5% to 20.649 GPa at 80°C, and further up 9.2% to 22.556 GPa at 100°C, achieving a total 21.9% gain, confirming the increase in the temperature at a steady rate to enhance the stiffness through steady-stage polymerization and reduction in the pores.

Likewise, 4GM1-2 follows the trend in the increase, from 25.678 GPa at 60°C to 28.803 GPa at 80°C (up 12.2%) and further to 31.002 GPa at 100°C (7.6% increase), achieving a total 20.7% increase in the modulus, confirming the mixture to gain from the thermal curing at the least shrinkage effect. However, 4GM1-3 first loses the stiffness at 80°C and later at 100°C, confirming the effect of the shrinkage in the beginning to be offset by the prolonged heat. 6M series, on the other hand, are less deterministic, in which the extreme modulus loss in 6GM1-1 is 38.6% at 100°C, indicating high alkalinity and high-curing temperature cause microcracking and structure relaxation, and in the 6GM1-4, the total gain in the modulus is 154.6%, indicating some formulation demands high heat-curing to attain optimum rigidity potential. The highest values of elasticity modulus were determined for 4GM1,5-1 and 6GM1.5-1, which showed an increase at 80°C and then a decrease at 100°C, which was probably due to microcrack formation due to thermal overstress, indicating that high molarity systems can achieve superior stiffness but are more prone to brittleness under extreme heat. Neupane et al. [21] pointed out the capacity of GBFS-GMs under modest thermal regimes to reach a modulus over 35 GPa thanks to the attainment of refined pore microstructures and dense C-A-S-H gel development. Lopes et al. [22] documented time-stabilization of elastic modulus in MK-based GMs at which the development of rigidity plateaued only upon extended ambient curing as a reflection of delayed but continuous ordering of the microstructure. Additionally, Kumar et al. [19] stressed that low-molarity mixes (4M and 6M) show modulus development as a function of curing temperature and Na_2SiO_3/NaOH proportion and thus implied optimization of rigidity would not depend as much on high alkalinity but on having very specific control of thermal and chemical variables.

The standards ASTM, Eurocode, ACI, and BS differ in their prediction accuracy, thus requiring specific assessment schemes for GMs. The ASTM values at 60 °C show a wide range of 1.18 MPa (1GM1-4) to 26.96 MPa (1GM1,5-2) and indicate the inconsistency of geopolymerization at early age. Eurocode underestimates strength because of the conservative approach based on typical cementitious

systems, whereas ACI overestimates strength following Portland trends rather than geopolymerization kinetics. Most samples show significant improvement at 80 °C, especially 1GM1-4 (+104.2%), demonstrating that moderate heat improves the binder structure and polymerization. However, the unexpected decrease of 1GM1-1 and 1GM1-3 (−41.9% and −39.5%) indicates that there was significant moisture loss, leading to increased porosity and internal cracking. The response at 100°C is more complex with 1GM1-4 showing an increase in strength of 333.1% indicating almost complete polymerization and matrix densification, while 1GM1-2 and 1GM1-3 show decreases in strength (-31.7% and -6.7%) probably due to microcracking caused by thermal stresses. ASTM has the most consistent testing findings, ACI overestimates strength increases and Eurocode is very conservative. The curing process reaches the maximum effectiveness at 80 °C, where the increase in strength and the reduction in shrinkage are balanced. The curing temperature of 100 °C should be utilized carefully to avoid the formation of structural flaws associated with moisture. 2M series also reflects temperature-dependent strength changes, where the ASTM strength from 60°C from 0.96 MPa (2GM1-4) to 20.57 MPa (2GM1,5-2). ACI overestimates strength, whereas the lowest strength is given by Eurocode for all the samples, similar to its trend for the 1M series. BS is moderate, agreeing closely with ASTM at lower temperatures but diverging at higher temps. The high variability at 60°C shows that the geopolymerization is not complete, causing differences in strength depending on the composition of the precursor and how well the activator works.

Increasing the temperature to 80°C favors 2GM1-2 (+115.7%) and 2GM1,5-1 (+39.9%); the evidence substantiates the assertion 80°C optimizes the dissolution in the silicates, the aluminas' mobility, and the kinetics in the polymerization. 2GM1-4, however, only minimally enhances (+14.6%), suggesting some mixes retain water in excess, and the rate in the reactions reduces. The most striking improvement comes in 2GM1,5-2 at 100°C to 30.3 MPa (ACI standard) from 73% improvement from the 60°C value, suggesting extended curing optimizes the connectivity in the gel in the geopolymer. 2GM1-2, however, declines from 23.23 MPa at 80°C to 18.55 MPa at 100°C, suggesting the overheating causes microcracking and shrinkage strains. The trends confirm the gain in the strength in the geopolymer follows a nonlinear trend, and the kinetics in the reactions, evaporation in the water, and the structure's densification interact dynamically. 2GM2,5-3, in particular, achieves one of the most striking improvement in the 100°C (+84.8%), suggesting the gelation in the high-silica precursors accelerates at the high temperature, and the mechanical response gets improved. 2GM1-4, however, at 100°C, only achieves 3.73 MPa (ASTM) and, by the same token, realizes the limitation in the design in the mixture.

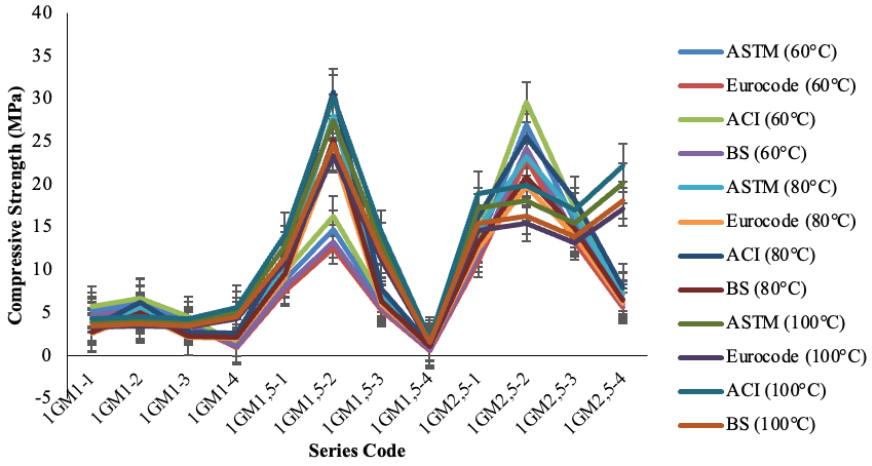
Overall findings confirm 80°C to be the optimal temperature in the balancing between the gain in the strength and the integrity in the microstructure, and 100°C to be useful only in the case of some mixes to provide additional energy to activate. 4M series also reiterates the intricate nature in the kinetics in the geopolymerization, the transformation in the structure, and the thermal effects, and the ASTM at 60°C from 4.17 MPa (4GM1-4) to 52.07 MPa (4GM1,5-1) The conservative nature of Eurocode underestimates strengths due to its reliance on empirical cement-based models, which fail to capture geopolymer formation mechanisms. ACI, however, overestimates strength (by ~10-15% over ASTM) and shows good agreement at elevated temperatures, but deviates significantly at lower curing temperatures. The strength improvement is mainly apparent in 4GM1,5-2 at 80°C with a 20% increase (52.14 MPa, ASTM), which confirms the idea that moderate heat is the best choice for an effective combination of geopolymerization kinetics and densification. However, 4GM1-4 has a less intense response (+28.3%) indicating a delayed polymerization which needs a longer or stronger cure. The data at 100°C shows two tendencies: (i) ongoing improvement in highly reactive systems, especially 4GM1-2 (+30.9%), due to better polycondensation and phase stabilization, and (ii) damage from shrinkage, illustrated by 4GM1-3 (~6% gain), where too much evaporation causes microstructural voids and interfacial weaknesses. ASTM is still the most experimental oriented standard. ACI's overestimations, especially at high temperatures (e.g., 62.84 MPa for 4GM2,5-2 (~10% higher than ASTM)), suggest the overcompensation of late reaction phases. Eurocode is conservative but gets better around 100°C, partly compensating for non-linear geopolymerization effects. The results confirm that 80°C is often the preferred temperature to balance fast strength development and durability, but that 100°C is necessary for some formulations that require more activation energy to complete polymerization. These discoveries are extended to the 6M series, showing the role of the interaction between the geopolymerization kinetics, precursor reactivity and thermal curing. The ASTM values at 60°C display a high variability in the mechanical behavior at early age with values ranging from 9.49 MPa (6GM1-4) to 41.65 MPa (6GM2.5-2) driven by the efficiency of aluminosilicate dissolution and the availability of alkali-ions. Eurocode has been found to underestimate strength (about 10-20% lower than ASTM), while ACI overestimates it (about 10-15% higher), especially for high strength mixtures, suggesting a mismatch with the nonlinear geopolymerization processes.

BS tracks ASTM quite closely, but is slightly underpredicting, especially at lower temperatures. At 80°C, a considerable increase in strength is found, especially in 6GM1-4 (+147%), reinforcing the function of thermal activation in promoting the production of Si-O-Al bonds and matrix densification. Similarly, 6GM1-2 reaches 50.61 MPa (ASTM), an increase of 28.1%, demonstrating that 80°C is the best compromise between reaction kinetics and structural integrity. However, abnormalities occur in GMs such as 6GM1-1, where strength decreases (-14.6%),

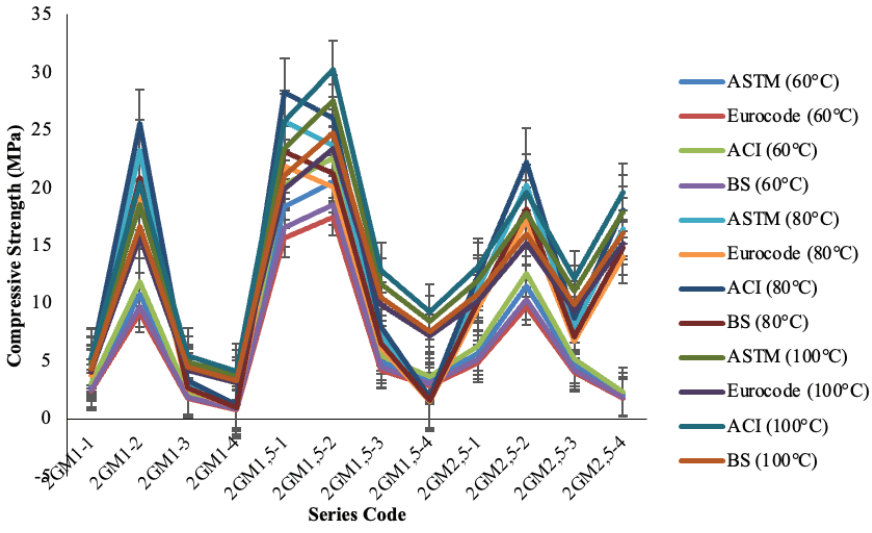
indicating that significant moisture loss in the early stages interferes with polymerization, causing microstructural inconsistencies. At 100 °C, the effects are twofold: (i) the further improvement of highly reactive formulations, e.g. 6GM2,5-2 (+45.7%, 58.96 MPa, ASTM), suggesting refined phase connectivity and reduced porosity; and (ii) stagnation or deterioration of thermally unstable mixes, e.g. 6GM1-1 (-43.7%), due to excessive shrinkage and interfacial microcracking affecting the final strength. ASTM is the most dependable standard for all temperatures. ACI overestimates (~12% more than ASTM at 100°C) and thus, less suitable for geopolymer systems. Eurocode does better at higher temperatures but is still conservative. BS is stable but slightly underestimates. These results indicate the high-temperature sensitivity of geopolymerization with 80°C being the optimum temperature for strength improvements while limiting the shrinkage concerns. Although selected items are heat-treated to 100°C, under extreme heat, defects are possible and heat treatment processes are required to condition them to achieve optimal lifespan and durability (Fig. 3).

The analysis of tensile/compressive (TS/CS) and flexural/compressive (FS/CS) strength ratios of the GMs (series 1GM1-1 to 6GM2,5-4) reveals significant differences in mechanical behavior, which are mainly influenced by the mix composition, activator/binder ratio and curing conditions (Fig. 4). The absence of fiber reinforcement in all the investigated samples emphasizes the direct importance of geopolymerization efficiency on mechanical performance. Factors including matrix densification, pore structure, and interparticle bonding are crucial in the formation of strength.

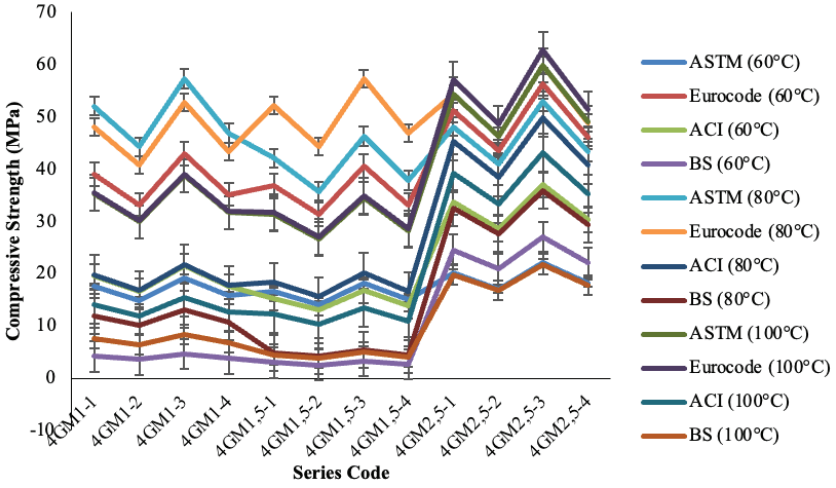
In the 1GM series the ratio of TS/CS (ASTM) varies from 0.1079 (1GM2,5-2) to 0.6424 (1GM1,5-4) while the Eurocode ratio varies from 0.1000 (1GM2,5-2) to 0.3287 (1GM1,5-4). However, the most mechanically resistant sample, 1GM1-4 (ASTM: 0.5155, Eurocode: 0.2839) shows much better tensile resistance. This is probably owing to optimal geopolymerization and hence a more cohesive



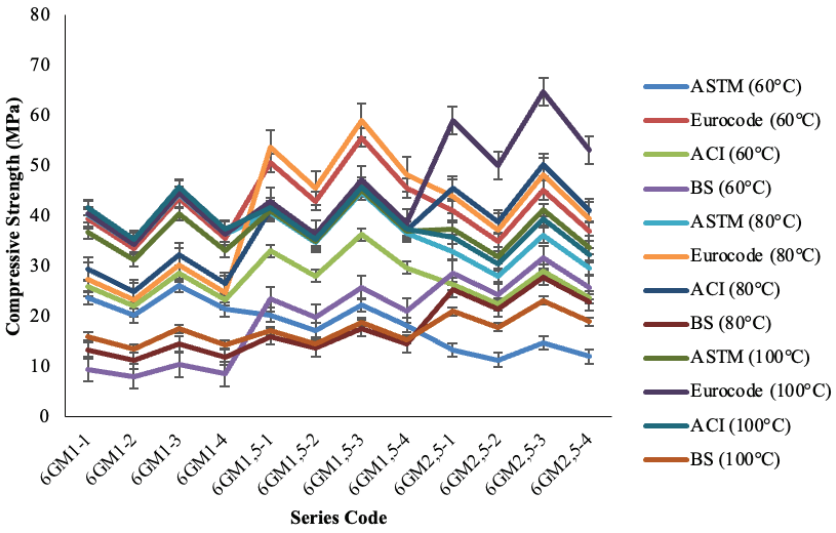
(a)



(b)

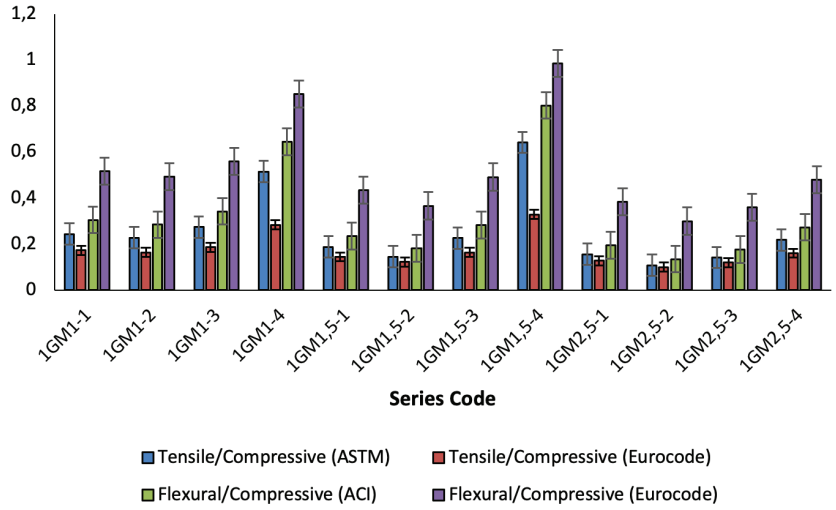


(c)

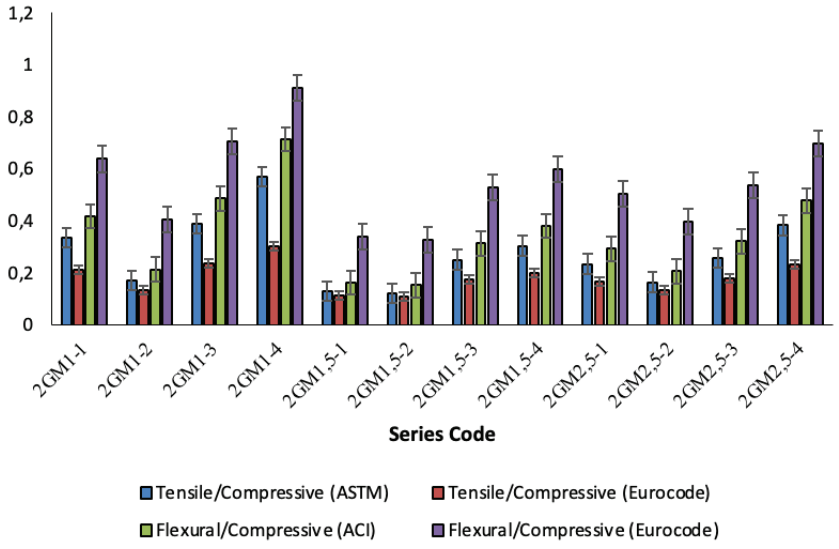


(d)

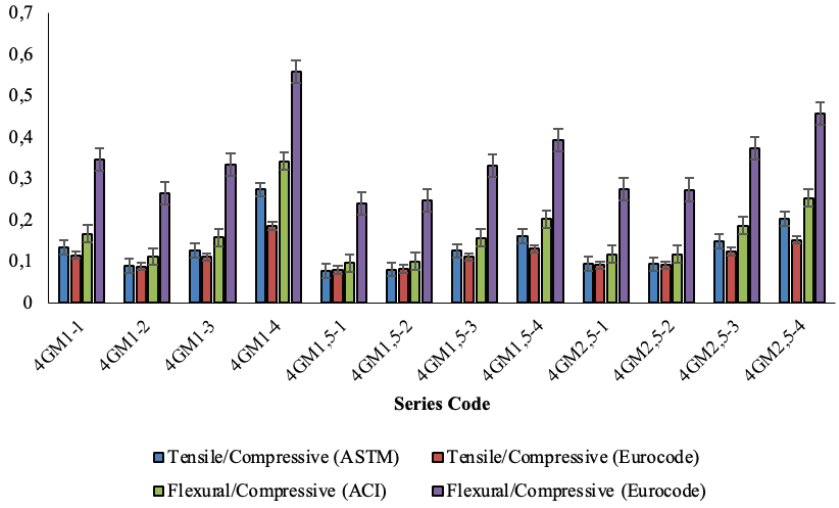
Figure 3. Compressive strengths of GMs prepared at different low-molarities and Na_2SiO_3/NaOH and mixing ratios according to international standards.



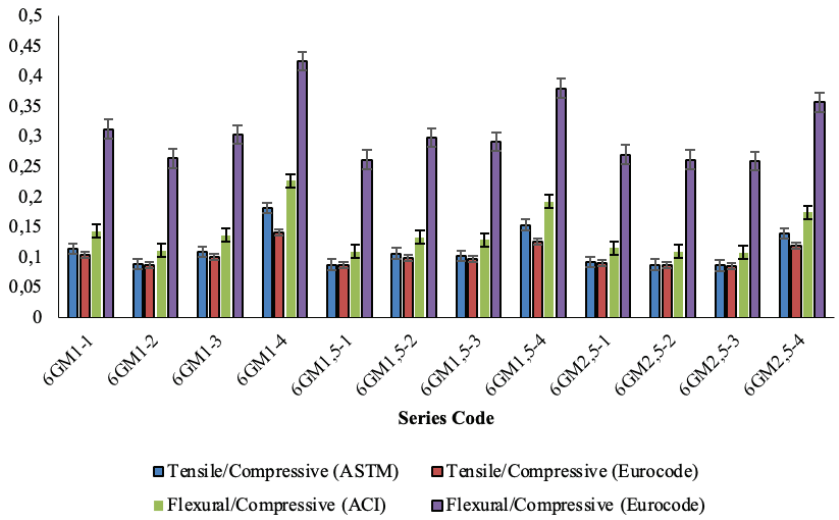
(a)



(b)



(c)



(d)

Figure 4. Flexural/Compressive strength and tensile/compressive strength of GMs prepared at different low-molarities and Na_2SiO_3/NaOH and mixing ratios according to international standards.

matrix with fewer unreacted particles. It implies that the activator-to-binder ratio was well balanced, which resulted in the complete breakdown of aluminosilicate precursors and a denser gel structure. Conversely, 1GM2.5-2 (ASTM: 0.1079, Eurocode: 0.1000) showed the lowest tensile performance, which indicates that the amount of activator was insufficient, the gel phase was not fully developed or the porosity was too high, all of which greatly decrease the tensile strength. FS/CS ratio (ACI and Eurocode) further supports these results as 1GM1,5-4 (ACI: 0.8029, Eurocode: 0.9862) has the maximum flexural strength which indicates a very continuous and well-bonded matrix which improves the efficiency of stress transmission. Conversely, 1GM2,5-2 (ACI: 0.1348, Eurocode: 0.3001) exhibits a brittle behavior under flexural loading, which can be attributed to poor interparticle adhesion and discontinuities in the microstructure. The TS/CS ratio (ASTM) of 2GM series is from 0.1235 (2GM1,5-2) to 0.5715 (2GM1-4); and the Eurocode ratio is from 0.1095 (2GM1,5-2) to 0.3041 (2GM1-4). Again 2GM1-4 (ASTM: 0.5715, Eurocode: 0.3041) is the strongest sample, perhaps because of a well designed alkali activation technique that allowed a complete geopolymerization and matrix consolidation.

Conversely, 2GM1,5-2 (ASTM: 0.1235, Eurocode: 0.1095) showed the lowest tensile capacity, potentially associated with an under-developed gel structure or an excess of residual porosity due to sub-optimal curing conditions. These tendencies are obeyed by the FS/CS ratio (ACI and Eurocode). 2GM1-4 (ACI: 0.7144, Eurocode: 0.9123) has a higher bending resistance, which means a stronger interparticle network and fewer stress concentration zones. In contrast, 2GM1,5-2 (ACI: 0.1543, Eurocode: 0.3285) has the worst flexural performance, indicating a heterogeneous microstructure sensitive to fracture initiation and quick failure under bending stresses. For the 4GM series, the TS/CS ratio (ASTM) is reduced to 0.0776 (4GM1,5-1) to 0.2742 (4GM1-4), while the Eurocode values are from 0.0803 (4GM1,5-1) to 0.1863 (4GM1-4), showing that these samples have a lower tensile capacity than the preceding series. Again, 4GM1-4 (ASTM: 0.2742, Eurocode: 0.1863) shows the highest performance, which may be attributed to a more favorable activator-binder balance, which enabled stronger gel formation and less porosity.

Conversely, 4GM1,5-1 (ASTM: 0.0776, Eurocode: 0.0803) has the lowest tensile response, which is probably caused by an under-polymerized network resulting in weak cohesion among particles. Regarding the FS/CS ratio, 4GM1-4 (ACI: 0.3427, Eurocode: 0.5591) is still better than the other GMs, meaning better features concerning stress distribution. Conversely, 4GM1,5-1 (ACI: 0.0970, Eurocode: 0.2410) has an extremely fragile flexural behavior, which suggests a material with rapid brittle fracture due to microstructural inhomogeneity. Similar trend is observed for 4GM2,5 series with TS/CS ratios ranging from 0.0939 (ASTM, 4GM2,5-2) to 0.2033 (ASTM, 4GM2,5-4) and Eurocode values from 0.0912 (4GM2,5-2) to 0.1526 (4GM2,5-4). Again, the poorest mechanical properties in this group indicate sub-optimal geopolymerization, increased residual porosity, and weaker interparticle interaction. The FS/CS ratios are generally low, with the highest values for 4GM2,5-4 (ACI: 0.2541, Eurocode: 0.4579), indicating slightly better flexural resilience than the other samples. However, 4GM2,5-2 (ACI: 0.1175, Eurocode: 0.2738) remains the most brittle mix probably due to limited diffusion of the activator and weak interfacial contacts between the geopolymeric phases. The 6GM series has the lowest overall mechanical performance with TS/CS ratios (ASTM) ranging from 0.0867 (6GM2,5-3) to 0.1818 (6GM1-4), and Eurocode values ranging from 0.0865 (6GM2,5-3) to 0.1417 (6GM1-4). These results indicate severe restrictions in matrix cohesiveness and overall strength growth, which may have stemmed from either an excess or deficiency of activator that hindered full polymerization. The best sample, 6GM1-4 (ASTM: 0.1818, Eurocode: 0.1417) has reasonable tensile strength, but is still considerably lower than the strongest samples from other series, which highlights the basic shortcomings of the mix design for the 6GM series. The 6GM2,5-3 (ASTM: 0.0867, Eurocode: 0.0865) had the worst tensile response, suggesting a highly porous discontinuous bonding material prone to brittle failure. The FS/CS ratio (ACI and Eurocode) further validates these results, as 6GM1-4 (ACI: 0.2272, Eurocode: 0.4251) exhibits the best flexural performance, possibly due to a slightly denser matrix facilitating better stress redistribution. Meanwhile, 6GM2,5-3 (ACI: 0.1084, Eurocode: 0.2596) is the least resistant of all, showing a considerable lack of adhesion between particles and microstructural integrity.

Multi-Criteria Decision-Making Method Application (HD Method) to Find the Best Solution

When reviewing literature or building decision support systems to make sense of experimental data, choosing the right evaluation approach is key. Most standard studies stick to single- or dual-parameter methods. A single-parameter setup evaluates results directly against a control group or similar published data—which is the route taken in the earlier sections of this paper. A dual-parameter approach takes things a step further by using correlation analysis to spot linear or non-linear relationships between two specific variables. Holistic evaluation, however, looks at the bigger picture. Instead of isolating variables, it factors every single parameter into the calculation at once, regardless of how many there are. This process typically yields a unified constant that serves as a reliable benchmark for pinpointing the best overall solution.

HD Method is one of the multi-criteria decision support methods and used to evaluate the alternatives and is used all parameters (see Appendix). The properties of the series used in the decision support steps were 7-days and 28-days of compressive strength, splitting tensile strength, direct tensile strength and ultrasound pulse velocity, 28-days of unit weight, water absorption and porosity (Table 5).

Table 5. Properties of samples used in the multi-criteria decision-support method

Series	fc, 7 days, MPa	fc, 28 days, MPa	fb, 7 days, MPa	fb, 28 days, MPa	fst, 28 days, MPa	ft, 28 days, MPa	d, g/cm^3	wa, %	p, %	UPV, 7 days, km/s	UPV, 28 days, km/s
Control	46.6	48.2	5.3	5.9	2.0	0.9	2.47	14.39	38.69	2793	2564
B4	51.2	54.4	7.1	7.8	2.6	0.9	2.48	9.41	25.71	2907	3012
B8	47.7	52.5	7.3	7.9	2.7	1.3	2.50	10.33	24.54	2884	2826
B12	45.5	49.2	8.5	9.2	3.0	1.8	2.51	11.92	23.00	1949	2264
P4	54.9	57.1	8.7	9.3	2.0	2.1	2.49	8.42	17.33	2732	3125
P8	55.3	58.6	9.5	9.7	2.6	2.4	2.55	9.96	20.24	2894	3322
P12	56.0	60.0	9.9	10.5	3.5	2.5	2.57	10.35	20.73	3058	3030

fc: Compressive Strength, fst: Splitting Tensile Strength, ft: Direct Tensile Strength,
UPV: Ultrasonic Pulse Velocity, d: Unit Weigth, wa: Water Absorption, p: Porosity.

*B-series refers to mixtures containing basalt fiber at 0.4% (B4), 0.8% (B8), and 1.2% (B12) by volume, while the P-series includes polyvinyl alcohol (PVA) fiber at the same volumetric ratios: 0.4% (P4), 0.8% (P8), and 1.2% (P12).

According to the HD Method results (Table 6), the mixtures of B12 and P12 were obtained as the best series in the groups regarding BF and PVAFs contents. On the other hand, the best of the bests in all GMs was determined and it was P12. Among the BF-reinforced GMs, B12 was an excellent candidate owing to the rigidity and high thermal stability of BFs, which contributed immensely towards its mechanical performance, especially its flexural (9.2 MPa) and splitting tensile strength (3.0 MPa), and its relatively low porosity (23.00%) and moderate UPV (2264 m/s). All these findings affirm that the BFs impart structural reinforcement and advanced stress transfer, especially in bending and tensile actions. Nevertheless, the ultimate excellence in P12 lies in the synergistic coupling among its microstructural densification, chemical activation system, and the fiber properties. When 1.2% PVAFs were used for reinforcement, the result was much superior mechanical, as well as durability, performance, such as compressive strength 60.0 MPa, flexural strength 10.5 MPa, splitting tensile strength 3.5 MPa, and higher UPV of 3058 m/s. The improved performance is attributed to multiple reasons, the first of which is that PVAFs facilitate uniform distribution of fibers and greater crack-bridging ability due to their hydrophilicity and interfacial bonding with the geopolymer matrix, thus reducing microcrack development and distribution of internal stresses better than basalt fibers. Second, PVAFs are thinner in diameter and less brittle, allowing them to interlock better with the gel structure and maintain their strength even with thermal shrinkage resulting from curing at 100 °C. Lastly, the high Na_2SiO_3/NaOH ratio of 2.5 with 6M NaOH in P12 induced superior polycondensation reactions, leading to a denser aluminosilicate network structure and improved pore refinement compared to B12. All these chemical and morphological benefits translated into reduced porosity (20.73% compared with 23.00%) and lower water absorption (10.35% compared with 11.92%) in P12, contributing directly towards its raised potential for durability in the longer term. Moreover, P12 exhibited the highest unit weight (2.57 g/cm^3), reflecting its superior packing density and matrix homogeneity. Although B12 certainly exhibited excellent response owing to the rigidity in basalt fibers, its internal structure was less cohesive, as evident in its lower UPV and high porosity. In contrast, P12 gained the benefit from both microstructural densification

Table 6. Multi-criteria decision-support method results

Mixture	*K**	The best in each group	The best of the bests
Control	1.000	-	-
B4	0.121	B12	P12
B8	0.099		
B12	0.039		
P4	0.025	P12	
P8	0.018		
P12	0.012		

** Lower is good*

Table 7. Properties of control and the best GM in the study

	fc, 7 days, MPa	fc, 28 days, MPa	fb, 7 days, MPa	fb, 28 days, MPa	fst, 28 days, MPa	ft, 28 days, MPa	d, g/cm^3	wa, %	p, %	UPV, 7 days, km/s	UPV, 28 days, km/s
Control	46.6	48.2	5.3	5.9	2.0	0.9	2.47	14.39	38.69	2793	2564
P12	56	60	9.9	10.5	3.5	2.5	2.57	10.35	20.73	3058	3030
	(+)	(+)	(+)	(+)	(+)	(+)	(+)	(+)	(+)	(+)	(+)

+ and – means the superiour and inferior, respectively.

and the reinforcement in its fibers, providing an optimized mechanical profile, enhanced environmental degradation, and better internal integrity. Thus, P12 not only ranked statistically as the best-performing mix in the HD analysis (lowest K value) but also showed overall superiority in mechanical, microstructural, and durability parameters.

The comparison of the properties of the control and P12 GMs was given in Table 7. Table 7 presented that P12 was superior to the control with 11 of 11 properties.

Sensitivity analysis of the compressive strength (fc) via thermal curing regimes (60 °C, 80 °C, and 100 °C) revealed salient insights into the thermal responsivity and compositional maturation of GMs, while the subsequent 28-day tests of fiber-reinforced specimens served to offer clearer understanding of the influence of fiber nature and dosage on mechanical maturation and reproducibility (Table 8). 1GM1,5-4, 2GM1,5-4, and 2GM2,5-4 series exhibited remarkably strong Δfcmax values (124–161%) due to retarded reaction kinetics at the lower temperatures and the existence of residual, or weakly polymerized, aluminosilicate phases which gel upon higher thermal input. Such late-stage maturation of the strength appears to result from extensive gel porosity and incomplete C-A-S-H/N-A-S-H polycondensation, corrected at 100 °C through compaction and better C-A-S-H/N-A-S-H backbone polymerization. Highly optimized mixes such as 6GM2,5-1 through 6GM2,5-3, conversely, exhibited low Δfcmax values (7–10%) as a reflection of early gel maturation and reduced susceptibility to higher-temperature thermal cure—a desirable property from a sustainability perspective, as these systems offer equivalent building permanence without the energy demands of the higher-temperature cure regimens. Uncharacteristic trends were observed in formulations 6GM1-1 ($\Delta fc_{80\rightarrow100}$ = –28.57%) and 4GM2,5-3 ($\Delta fc_{80\rightarrow100}$ = 180%), likely arising from the conflicting effects of excessive

Table 8. Sensitivity analysis of compressive strength (fc) in GMs

Series	Δfc (60=>80 (%))	Δfc (80=>100 (%))	Δfc_{max} (%)
1GM1-1	-9.09	-6.00	15.79
1GM1-2	-6.67	-25.00	34.18
1GM1-3	-3.64	-15.09	19.61
1GM1-4	-7.89	-5.71	14.15
1GM1,5-1	31.43	5.07	30.93
1GM1,5-2	36.59	-1.79	29.61
1GM1,5-3	23.08	62.50	70.91
1GM1,5-4	22.22	286.36	160.80
1GM2,5-1	23.68	7.45	27.68
1GM2,5-2	15.22	-5.66	14.09
1GM2,5-3	8.82	-3.78	8.44
1GM2,5-4	8.33	76.92	68.75
2GM1-1	42.86	-16.00	35.43
2GM1-2	162.00	-23.66	86.48
2GM1-3	20.00	10.00	27.27
2GM1-4	100.00	10.00	69.23
2GM1,5-1	33.33	6.25	33.33
2GM1,5-2	29.27	7.55	31.79
2GM1,5-3	36.00	27.45	53.75
2GM1,5-4	42.86	212.50	150.78

Table 8. Sensitivity analysis of compressive strength (fc) in GMs (continued)

Series	Δfc (60=>80 (%))	Δfc (80=>100 (%))	Δfc_{max} (%)
2GM2,5-1	33.33	21.43	46.99
2GM2,5-2	8.11	10.00	17.36
2GM2.5-3	31.25	14.29	39.34
2GM2.5-4	47.62	133.87	124.10
4GM1-1	11.11	10.00	20.00
4GM1-2	14.29	30.00	40.16
4GM1-3	27.27	17.86	39.76
4GM1-4	20.00	33.33	47.37
4GM1,5-1	-3.85	8.00	7.69
4GM1,5-2	8.33	7.69	15.38
4GM1,5-3	-14.29	44.44	36.92
4GM1,5-4	-25.00	77.78	56.76
4GM2,5-1	-10.53	61.76	49.61
4GM2,5-2	-9.59	75.76	58.82
4GM2,5-3	-23.08	180.00	105.88
4GM2,5-4	-13.64	121.05	83.13
6GM1-1	16.67	-28.57	33.33
6GM1-2	31.58	-10.00	27.07
6GM1-3	28.57	-8.33	24.74
6GM1-4	40.00	-14.29	33.33
6GM1,5-1	5.00	-28.57	32.14
6GM1.5-2	25.58	-7.41	22.45
6GM1,5-3	6.82	-17.02	18.46
6GM1,5-4	38.89	-12.00	32.31
6GM2,5-1	10.00	-6.82	9.60
6GM2,5-2	4.76	-6.82	7.09
6GM,.5-3	2.44	-9.52	9.92
6GM2,5-4	11.11	15.00	24.59

Series	fc (28d, MPa)	Δfc (7–28d) [%]	Δfb (7–28d) [%]	fc Error Margin (CoV %)
Control	48.2	3.43	11.32	2.07
B4	54.4	6.25	9.86	1.84
B8	52.5	10.06	8.22	1.90
B12	49.2	8.13	8.24	2.03
P4	57.1	4.01	6.90	1.75
P8	58.6	5.97	2.11	1.71
P12	60.0	7.14	6.06	1.67

thermal exposure—manifesting as microcracking and vapor-induced porosity—and delayed onset of effective geopolymerization. Thermal activation effects are nonlinear and highly composition-driven, as a consequence of the interactions of ion migrability, precursor reactivity, moisture transfer, and gel evolution channels. As a complement to the thermal characterization, the fiber-reinforced GMs exhibited varied strength and consistency responses. For the basalt fiber mixes (B4, B8, B12), the B8 exhibited the maximum compressive strength gain (Δfc = 10.06%) as a consequence of the optimized balance of the fiber distribution and matrix compatibility for the medium dosages, though with modest flexural strength maturation. For the polyvinyl-based mixes (P4, P8, P12) the 28-day compressive strengths reached higher values (up to 60 MPa for the P12) with extraordinary reproducibility (CoV = 1.67%) as a consequence of homogeneous incorporation of the fibers and stable crack-bridging efficacy. P8 exhibited a noticeably low flexural gain (Δfb = 2.11%) as a consequence of likely saturation of the toughness effect at the earliest maturation stage, while B12 exhibited proportional growth for both the compressive and bending arenas, though with heightened variability. Overall, the findings emphasize that thermal and mechanical optimization in GMs must address not only strength development but also processing energy efficiency and statistical consistency. Fiber type and dosage critically influence both performance

magnitude and its reliability, with P-series outperforming B-series in uniformity, while sensitivity trends from unreinforced specimens illuminate the necessity for tailored curing regimes based on molarity, precursor selection, and desired application conditions.

CONCLUSION

1. This research systematically investigated the influence of selected parameters NaOH concentration, Na_2SiO_3/NaOH ratio, type and content of fibers, and curing temperature upon the mechanical and physical performance of GMs. The objective involved the design and optimization of GMs with the help of GBFS and CWP under low-alkali activation with the aim of producing sustainable substitutes with high strengths to OPC-based materials. In addition to performance analysis, the study also applied a multi-criteria decision analysis technique to select the best mix design with balanced strength, durability and structural performance.
2. The molarity of the activator significantly affected the efficiency of the geopolymerization process. The 1M and 2M mixtures showed a higher porosity, with an incomplete polymerization process, whereas 4M and 6M resulted in a denser and more homogeneous matrix with enhanced mechanical properties. The results indicated that the Na2SiO3/NaOH ratio of 2.5 was optimal, promoting better silicate polymerization and increasing matrix compactness.
3. The highest CS was 58.96 MPa recorded in the 6M2,5-2 series at 100 °C. In contrast, GMs in 1M lost 41.9% of their strength from 5.25 MPa at 60 °C to 3.05 MPa at 80 °C before their strength increased slightly at 100 °C, but in 2M they gained 72.2% strength at 80°C, but decreased by 20.1% at 100 °C.
4. Modulus of elasticity was directly correlated with the curing temperature and activator concentration, with the highest values recorded in 4M and 6M-GMs, increasing by 20.7% at 100 °C compared to 60 °C curing. In 1M, GMs decreased by 23.8% at 80 °C, while it partially increased at 100 °C, but in 6M, a 38.6% decrease occurred at 100 °C.
5. FS/CS ratio was lowest for 1M and 2M mixes (0.1079-0.3287) primarily because of ineffective polymeric bonding caused by insufficient precursor dissolution, hindered polycondensation, and discontinuous gelation. Consequently, N-A-S-H or C-A-S-H connectivity, porosity, and interparticle bridge strength were all weak, undercutting tensile stress redistribution and enabling matrix-filler interfacial crack initiation. In contrast, 4M-activated GMs exhibited the stablest FS/CS ratio (peaking at 0.5591 at 100 °C) as a pointer to a fully developed, dense gel matrix with higher cohesion, lower porosity, and stronger matrix-aggregate bonds, all better equipped to endure flexural loads.
6. TS/CS ratio followed a similar trend with the highest value being found in 1GM1-4 (1M NaOH, 80°C curing) (0.5155) and the lowest value being found in 1GM2.5-2 (Na_2SiO_3/NaOH:2.5, 60 °C curing) (0.1079).
7. Standardized strength predictions exhibited variations across different models. ASTM showed the best agreement with the experimental data. The ACI predictions tended to underestimate the compressive strength by 10-15% for the high molarity mixes, which may be attributed to discrepancies in the underlying assumptions about the behavior of the material. Eurocode was always predicting conservatively, Strength was underestimated by 5-20% which can be explained by Eurocode's focus on safety aspects. These differences can largely be attributed to the different concepts and local variations in the development of these standards. ACI 318, for example, is specific to traditional OPC-based concrete in North American settings, and applies rather conservative reduction factors, especially for mixes with unknown chemistries, for example, such as alkali-activated binders or high-molarity GMs. Consequently, it always underestimates the compressive strength, especially for heat-cured, high-reactivity mixtures. Likewise, while BS standards agree closer with ASTM at lower curing temperatures, it is more sensitive towards curing-induced dimensional instabilities—such as shrinkage and thermal microcracking—which become stronger at higher temperatures such as 100 °C. Conversely, Eurocode provides a more balanced and solid prediction model that, although it experiences some underestimations, is always closer in agreement with experimental outcomes for all curing conditions and all molarity values. This is presumably because Eurocode is semi-probabilistic in nature, uses wider calibration dataset, and treats mechanical parameters such as characteristic strength class, creep, shrinkage, and long-term deformations in greater detail. Moreover, Eurocode incorporates partial safety factors that are flexible with respect to disparate structural and material conditions, rendering it especially adoptive towards novel binder systems such as GMs. In the current work, while point-wise accurate predictions were achieved using ASTM for distinct conditions, Eurocode showed consistency in proximity for wide-ranging variables, which justifies its title as the most accurate model in the systemic engineering design standpoint.
8. P12 series, identified as the best performing GM by HD Method and with the lowest K value (0.012), outperformed the control in all 11 parameters while demonstrating higher compressive (↑24.5%, 60.0 MPa), flexural (↑77.9%, 10.5 MPa), splitting tensile (↑75%, 3.5 MPa) and direct tensile strength (↑177.8%, 2.5 MPa) strength, proving its superior performance.
9. Regarding durability and structural integrity, P12 achieved the lowest water absorption (10.35%) – a 28% reduction compared to the control (14.39%) – and

significantly lower porosity (20.73%) compared to 38.69% of the control, improving resistance to aggressive environmental conditions. Furthermore, P12 had the highest unit weight of all mixes (2.57 g/cm^3), indicating a denser, more compact structure, and UPVs confirmed P12's internal homogeneity with values of 3058 m/s (7 days) and 3030 m/s (28 days), while significantly outperforming the control (2793 m/s and 2564 m/s, respectively).

10. The practical application of these findings is their straightforward correlation with long-term durability under conditions of practical exposure. The deep reduction in water absorption and porosity in P12, known not only as an indicator of lowered permeability, but also points towards an extensively developed, cross-linked network of aluminosilicate, which actively restricts the migration of aggressive substances such as chlorides, sulfates, and carbon dioxide. The pore structure refinement eliminates the threat of internal modes of degradation such as steel corrosion, freeze–thaw spalling, and chemical attack, typical in infrastructures exposed to seashore or varying environments. In addition, the unusually high UPVs indicate enhanced internal coherence and few microstructural discontinuities, a non-destructive indicator of compactness and crack-growth resistivity. As important as this is, the increase in the unit weight, an indicator reflecting the amount of microstructural densification achieved through complete polycondensation and efficient void-filling through reaction products. The densification is no passive by-product, but physical proof of enhanced chemical bonding and decreased entrained air, producing a more rigid and homogeneous matrix. Combined, these features make P12 a structurally stable and chemical-resistant material, competitive in cases demanding prolonged service life and aggressive environmental conditions, far beyond those predicted by strength parameters alone.
11. To ensure the global applicability and conformity to regulations of the anticipated low-alkaline geopolymer mortar, specifically the P12 series, a comparison investigation was conducted against available international standards, design codes, and environmental certification procedures that now mandate sustainable building techniques. In the European Union, the Level(s) scheme (European Commission, 2020)—the EU's Green Deal and Fit for 55 Package's reporting tool—attains a maximum 300 kg CO_2-eq/m^3 cradle-to-gate Global Warming Potential (GWP) limit level suitable for structural-grade concreets (Indicator 1.2: Life Cycle GWP). As in this paper 100% waste-based binders (75% GBFS and 25% CWP) and medium activator levels (6M NaOH and 2.5 Na_2SiO_3/NaOH ratio) were employed, corresponding GWP amounts conform to past life cycle results that have revealed 70–85% CO_2 savings per OPC-based [23-25]. Furthermore, Eurocode 2 (EN 1992-1-1:2004) imposes structural concrete classification parameters based on characteristic mean compressive strength and exposure classes (e.g., XC3 being level of carbonation in moderate humidity, XD2 level of chloride in humid areas, XF2 freeze-thaw with de-icing) and requires not only 50 MPa and over compressive strength but also low permeability and volume stability resistance to shrinkage-induced cracks as well.
12. Within occupational and environmental safety considerations, through Green Building Evaluation Standard GB/T 51231-2016 and its antecedent GB/T 29431-2012, maximum allowable dosages are stipulated for alkali (typically <10 wt% Na_2Oeq) to avert hazards of efflorescence, handling risk, and microcracking. The available formulations, employing NaOH at 6M (~5.4 wt% Na_2Oeq assuming complete dissociation), are significantly lower and therefore below such a threshold, and hence, the mortar system complies with these safety guidelines. Moreover, such a level of alkali content is also in confluence with the REACH regulation via EC No. 1907/2006 by establishing a threshold to workplace exposures of corrosive alkaline products employed in European applications in industries. In America, under Materials & Resources – Building Product Disclosure and Optimization (MR-BPDO) credit, the LEED v4.1 rating scheme (USGBC, 2020) rewards performance-based points to products that have Environmental Product Declarations (EPDs) displaying GWP saving ≥20% over industry baseline. With complete avoidance of OPC and kiln-based precursors in mortars subject to study, and superior mechanical-to-porosity fractions, a mix is qualified for high-scoring EPD profiles. Low permeability and ultra-high UPV (all > 3000 m/s) also complies with LEED EQc4 prerequisites under Indoor Environmental Quality by curbing emissions due to alkali, and it meets BREEAM's Hea 02 Indoor Air Quality and Mat 03 Responsible Sourcing credits (BRE, 2021). At a structural level, 0.5591 and 0.1818 FS/CS and TS/CS ratios in P12 represent internally optimized bonding conditions, in conformance with tension-to-compression ratios usually reported in EN 206 and EN 12390-3/6 standard-class C50/60 concretes. These are, in comparison with ACI 318-19 empirical models (subject to a tendency to underestimate tensile strength in GMs, further indications favoring model updates when proceeding from OPC-based to GMs (ACI CODE-318, 2022). Notably, ASTM C494 and C1012 durability categories (e.g., sulfate resistance, expansion limitation) are also fulfilled indirectly through observed porosity and gel densification trends that are leading long-term chemical resistance predictors in aggressive exposures. In addition, the use of an HD multiple-criteria decision-support framework employed in these pages is a mirror image of decision matrices employed by Singapore's Green Mark and Australia's Green Star schemes that prioritize whole-system environmental and durability performance over single strength parameters. Consequently, as such, it not only indicates a low-carbon material substitute but

also shows an engineeringly prudent, code-compatible, and lifecycle-conscious binder system demonstrably congruent with international green building mandates and structural safety tenets.

13. These findings go beyond ordinary lab-scale material synthesis and redefine the low-molarity geopolymer mortars as not only experimental materials but also industrially scalable and viable industrial responses to the global infrastructure demand that is resource-resilient and decarbonized. The novel alkali activation processes devised in this research—with the employment of low-molar solutions of NaOH, optimized mass silicate-to-hydroxide mass ratios, and the effective valorization of granulated blast furnace slag and ceramic dust—present a rational framework for industrial up-scaling that is a trade-off between economic feasibility and operational security and environmental responsibility. Compared to traditional high-molarity systems typically involving high chemical expenses, toxicity hazard, specialized storage needs, and workplace hazard, these low-alkali formulations are essentially compatible with current commercial concrete batching facilities, heat curing systems, and decentralized/module-based production facilities in resource-limited areas. This compatibility obviates the necessity for costly infrastructural retrofitting facilities and enables these mixes to serve as drop-in substitutes within current production operations.
14. From an economical standpoint, the substitution of OPC, which makes up over 90% of the binder-related carbon emissions in ordinary mortars, has the advantage of lower raw material costs and the removal of carbon penalties from calcination and clinkerization. Moreover, utilizing industrial by-products that would otherwise be disposed of or employed as low-value applications, helps to transform trash into high-performance construction materials, in accordance with the ideas of industrial symbiosis and circular economy. The benefits are much more pronounced from a life cycle perspective. The improved durability performance achieved, lower porosity and increased crack growth resistance, leads to a longer service life and lower maintenance requirements, giving significant long term cost savings. An extra advantage is that the moderate heat curing regime used (60–100 °C) with 80 °C being the optimal, is compatible with renewable and low grade heat sources such as geothermal projects, biomass boilers or solar thermal units. This allows a net energy input during cure to be lowered as part of a strategy for minimizing overall embodied energy.
15. Environmentally, the total exclusion of OPC and the application of inert and reactive industrial waste precursors lead to an enormous reduction in emissions—by an estimated 70–90% depending upon the baseline case—while at the same time averting landfilling and endorsing waste diversion measures. From a regulatory perspective, the formulated system obtains its strength and modulus of elasticity within the predictive bands of ASTM and BS specifications. This conformity enables simpler certification procedures, compatibility with construction code requirements, and wider market acceptance—issues which often hinder the practical field application of novel cementitious materials. As an integrated whole, the proffered low-molar geopolymer system falls at the crossing point between economic feasibility, ecological accountability, and structural performance reliability. It embodies a degree of techno-scientific maturity that is higher than experimental possibility but within the scope of buildable, code-compatible material solutions that are commercially investable. Within a world in which infrastructure systems are confronted with the imperative to decarbonize under mounting pressure while conceding little to no loss in systemic resilience, this investigation posits a durable model for scalable material innovation. Not only does it redefine what sustainable concrete can constitute, but also how and under what circumstances it can be produced and deployed. Future research can entail techno-economic appraisal, piloting at the field scale with subsequent integration into digital twin environments for predictive modeling under actual service conditions. Even so, existing results already constitute sound evidence that such systems are no longer a possibility, but are feasible, attractive, and necessary.

ACKNOWLEDGMENTS

The development of the Holistic Decision (HD) method was funded by the Van Yüzüncü Yıl University Research Fund. The authors are deeply grateful to the Scientific Research Projects Coordination Unit for supporting this research. (Project number: FYD-2021-9379).

AUTHORSHIP CONTRIBUTIONS

Authors equally contributed to this work.

DATA AVAILABILITY STATEMENT

The authors confirm that the data that supports the findings of this study are available within the article. Raw data that support the finding of this study are available from the corresponding author, upon reasonable request.

CONFLICT OF INTEREST

The authors declared no potential conflicts of interest with respect to the research, authorship, and/or publication of this article.

ETHICS

There are no ethical issues with the publication of this manuscript.

STATEMENT ON THE USE OF ARTIFICIAL INTELLIGENCE

Artificial intelligence was not used in the preparation of the article.

REFERENCES

[1] Asteris PG, Apostolopoulou M, Skentou AD, Moropoulou A. Application of artificial neural networks for the prediction of the compressive strength of cement-based mortars. Comput Concr 2019;24:329–345.

[2] Al-Chaar G, Abu-Hamdan M, Ulmen B. Natural pozzolan as a partial substitute for cement in concrete. Open Constr Build Technol J 2013;7:33–42. [CrossRef]

[3] Apostolopoulou M, Asteris PG, Armaghani DJ, Douvika MG, Lourenço PB, Cavaleri L, et al. Mapping and holistic design of natural hydraulic lime mortars. Cem Concr Res 2020;136:106167. [CrossRef]

[4] Durastanti C, Moretti L. Environmental impacts of cement production: a statistical analysis. Appl Sci 2020;10:8212. [CrossRef]

[5] Davidovits J. Geopolymer chemistry and applications. 4th ed. Saint-Quentin: Institute for Geopolymer Science & Technology; 2013.

[6] Deb PS, Nath P, Kumar S. The effects of ground granulated blast-furnace slag blending with fly ash and activator content on the workability and strength properties of geopolymer concrete cured at ambient temperature. Mater Des 2014;62:32–39. [CrossRef]

[7] Fang G, Kei HW, Wenlin T, Zhang M. Workability and mechanical properties of alkali-activated fly ash slag concrete cured at ambient temperature. Constr Build Mater 2018;172:476–487. [CrossRef]

[8] Aliabdo A, Elmoaty A, Mohammed E. Factors affecting the mechanical properties of alkali activated ground granulated blast furnace slag concrete. Constr Build Mater 2019;197:339–355. [CrossRef]

[9] Gupta A. Investigation of the strength of ground granulated blast furnace slag based geopolymer composite with silica fume. Mater Today Proc 2021;44:23–28. [CrossRef]

[10] Luhar I, Luhar S, Abdullah MMAB, Nabiałek M, Sandu AV, Szmidla J, et al. Assessment of the suitability of ceramic waste in geopolymer composites: an appraisal. Materials (Basel) 2021;14:3279. [CrossRef]

[11] Ricciotti L, Occhicone A, Ferone C, Cioffi R, Tarallo O, Roviello G. Development of geopolymer-based materials with ceramic waste for artistic and restoration applications. Materials (Basel) 2022;15:8600. [CrossRef]

[12] Zhang GY, Bae SC, Lin RS, Wang XY. Effect of waste ceramic powder on the properties of alkali-activated slag and fly ash pastes exposed to high temperature. Polymers (Basel) 2021;13:3797. [CrossRef]

[13] Kaya M. Mechanical properties of ceramic powder based geopolymer mortars. Mag Civ Eng 2022;112:11207.

[14] Coban O, Akgul T. Evaluation of some mechanical and physical properties of sodium hydroxide (NaOH) activated tile waste geopolymer mortars. Pamukkale Univ J Eng Sci 2025;31:116–124. [CrossRef]

[15] Kumar VS, Ganesan N, Indira PV. Effect of molarity of sodium hydroxide and curing method on the compressive strength of ternary blend geopolymer concrete. IOP Conf Ser Earth Environ Sci 2017;80:012011. [CrossRef]

[16] Kop M, Yazıcıoglu S. Mechanical properties of fly ash and blast furnace slag based geopolymer mortars in thermal curing environment. Gazi Univ J Sci C Des Technol 2023;11:756–765. [CrossRef]

[17] Kabay N, Kızılkanat AB. A comparative study on the thermal performance of mortars with different formulations. Sigma J Eng Nat Sci 2020;38:183–189.

[18] Al-Zwainy F, Al-Marsomi M. Structural equation modeling of critical success factors in the programs of development regional. J Proj Manag 2023;8:119–132. [CrossRef]

[19] Kumar M, Kumar A, Solanki D, Mungule M. Low molarity geopolymer concrete: effects on compressive strength, elastic modulus, sorptivity and chloride migration. Constr Build Mater 2023;409:134065. [CrossRef]

[20] Bilondi MP, Ghaffarian V, Daluee MA, Pakizehrooh R, Tazik SH, Behzadian A, et al. Experimental studies on mix design and properties of ceramic-glass geopolymer mortars using response surface methodology. Sci Rep 2025;15:282. [CrossRef]

[21] Neupane K, Chalmers D, Kidd P. High-strength geopolymer concrete: properties, advantages and challenges. Adv Mater 2018;7:15–25. [CrossRef]

[22] Lopes A, Lopes S, Fernandes M. Time evolution of the modulus of elasticity of metakaolin-based geopolymer. Appl Sci 2023;13:2179. [CrossRef]

[23] Dollente IJR, Tan RR, Promentilla MAB. Life cycle assessment of precast geopolymer products. Chem Eng Trans 2021;88:799–804.

[24] Martínez A, Miller SA. Life cycle assessment and production cost of geopolymer concrete: a meta-analysis. Resour Conserv Recycl 2025;215:108018. [CrossRef]

[25] Wudil YS, Al-Fakih A, Al-Osta MA, Gondal MA. Effective carbon footprint assessment strategy in fly ash geopolymer concrete based on adaptive boosting learning techniques. Environ Res 2025;266:120570. [CrossRef]

APPENDIX

When you're trying to make sense of experimental data—whether you're reviewing literature or using decision support tools—a holistic evaluation approach makes life a lot easier. Instead of looking at variables one by one, it takes every single parameter into account all at once, no matter how many you have. The math usually boils down to a single constant, which gives you a clear baseline to figure out the best overall option. The Holistic Decision (HD) method is a great real-world example of this in multi-criteria decision-making. Instead of focusing on just one isolated result, it brings all your chosen physical, mechanical, and durability traits together so you can see how an alternative mixture actually performs as a whole. By running the data through simple normalization and aggregation steps, it avoids over-optimizing for just one factor and lands on the most balanced solution—giving each alternative a single overall performance index, known as the K value.

Parameters of alternatives are presented in the alternatives' matrix (Eq. A1).

$$M = \begin{bmatrix} m_{11} & \cdots & m_{1l} \\ \vdots & \ddots & \vdots \\ m_{k1} & \cdots & m_{kl} \end{bmatrix} \tag{A1}$$

where m_{kl} is the l^{th} criterion of k^{th} alternative, and M is the score matrix of alternatives.

Parameter normalization depends on whether a control baseline is present in the database. When a control exists, the alternative parameters are normalized by dividing them directly by the corresponding control value. Without a control, the standard approach is to calculate the parameter mean, multiply it by an incrementing scaling factor (e.g., 2, 3, etc.), and divide the alternatives by this scaled mean. However, rather than using the mean, it is recommended to select a baseline value that exceeds twice the maximum parameter value (Eq. A2).

$$M_d = \begin{bmatrix} m_{11}/m_{11} & \cdots & m_{1l}/m_{1l} \\ \vdots & \ddots & \vdots \\ m_{k1}/m_{11} & \cdots & m_{kl}/m_{1l} \end{bmatrix} = \begin{bmatrix} 1 & \cdots & 1 \\ \vdots & \ddots & \vdots \\ d_{k1} & \cdots & d_{kl} \end{bmatrix} \tag{A2}$$

where M_d is the relative criterion matrix of alternatives and d_{kl} is the l^{th} relative criterion of k^{th} alternative.

Then, if weighing of the parameters is intended, the relative parameters are multiplied by the weights of the parameters (Eq. A3).

$$M^* = \begin{matrix} w \\ \vdots \\ w_n \end{matrix} \begin{bmatrix} m_{11} & \cdots & m_{1l} \\ \vdots & \ddots & \vdots \\ m_{k1} & \cdots & m_{kl} \end{bmatrix} = \begin{bmatrix} m^*_{11} & \cdots & m^*_{1l} \\ \vdots & \ddots & \vdots \\ m^*_{k1} & \cdots & m^*_{kl} \end{bmatrix} \tag{A3}$$

where M^* is the score matrix of alternatives, and m_{kl} is the l^{th} weighted criterion of k^{th} alternative.

In the final step, a scalar value (K) is calculated for each alternative using a fractional formula. The numerator multiplies the relative parameters that are less than 1.0, while the denominator does the same for parameters greater than 1.0. Once all K values are worked out, they are ranked from lowest to highest, with the lowest \$K\$ representing the best choice. Finally, the acceptability levels (ALs) for each alternative can be calculated using the minimum (K_{low}) and maximum (K_{high}) values across the dataset.

The difference (ΔK) between the highest and lowest K values is divided by four to establish four distinct performance tiers: Excellent, Very Good, Good, and Acceptable.

The alternative is "excellent", if $(0\times\Delta K + K_{low}) \leq K < (0.25\times\Delta K + K_{low})$,

The alternative is "very good", if $(0.25\times\Delta K + K_{low}) \leq K < (0.50\times\Delta K + K_{low})$,

The alternative is "good", if $(0.50\times\Delta K + K_{low}) \leq K < (0.75\times\Delta K + K_{low})$,

The alternative is "acceptable", if $(0.75\times\Delta K + K_{low}) \leq K \leq (1.00\times\Delta K + K_{low})$, compared to desired/control alternative.